Earth and Planetary Science Letters 353-354 (2012) 253–269

Contents lists available at SciVerse ScienceDirect

Earth and Planetary Science Letters

journal homepage: www.elsevier.com/locate/epsl

Reconciling dynamic and seismic models of Earth's lower mantle: The dominant role of thermal heterogeneity

D. Rhodri Davies [a,*], S. Goes [a], J.H. Davies [b], B.S.A. Schuberth [c], H.-P. Bunge [d], J. Ritsema [e]

[a] Department of Earth Science and Engineering, Imperial College London, London, UK
[b] School of Earth and Ocean Sciences, Cardiff University, Cardiff, UK
[c] Université de Nice Sophia-Antipolis, Centre National de la Recherche Scientifique, Observatoire de la Côte d'Azur, Géoazur, France
[d] Department of Earth and Environmental Sciences, Ludwig–Maximilians–Universitat, Munich, Germany
[e] Department of Geological Sciences, University of Michigan, Ann Arbor, USA

ARTICLE INFO

Article history:
Received 5 April 2012
Received in revised form
24 July 2012
Accepted 13 August 2012
Editor: Y. Ricard
Available online 26 September 2012

Keywords:
Earth structure
seismic heterogeneity
seismic tomography
mantle dynamics
mantle composition
plumes

ABSTRACT

Two large low-shear-velocity provinces (LLSVPs) in the deep mantle beneath Africa and the Pacific are generally interpreted as hot but chemically dense 'piles', which have remained isolated from mantle circulation for several hundred million years. This interpretation largely hinges on four seismic observations: (i) their shear wave velocity anomalies are considered too large for purely thermal structures; (ii) shear wave velocity gradients at their edges are sharp; (iii) their shear to compressional wave-speed anomaly ratios are high; and (iv) their shear and bulk-sound velocity anomalies appear to be anti-correlated. However, using compressible global mantle circulation models driven by 300 Myr of plate motion history and thermodynamic methods for converting from physical to seismic structure, we show that observed lower mantle shear wave velocity anomalies do not require, and are most likely incompatible with, large-scale chemical 'piles'. A prescribed core-mantle-boundary temperature of 4000 K, which is consistent with current estimates, combined with anelastic seismic sensitivity to temperature, ensures that purely thermal LLSVPs, strongly focussed beneath Africa and the Pacific by subduction history, can reconcile observed shear wave velocity anomalies and gradients. By contrast, shear wave velocity anomalies from models that include dense chemical 'piles' at the base of Earth's mantle, where 'piles' correspond to only 3% of the mantle's volume, are substantially stronger than the tomographic model S40RTS, even after accounting for limited tomographic resolution. Our results also suggest that in the presence of post-perovskite, elevated ratios between shear and compressional wave-speed anomalies and the correlation between shear and bulk-sound velocity anomalies cannot be used to discriminate between thermal and compositional heterogeneity at depth: in all calculations, an anti-correlation only occurs within the post-perovskite stability field. Taken together, this implies that although there must be considerable chemical heterogeneity within Earth's mantle, large, coherent 'piles' are not required to reconcile the seismic observations examined here. Indeed, our results suggest that if chemical heterogeneity is present in these regions, its dynamical and seismic significance is far less than has previously been inferred.

1. Introduction and motivation

It has long been recognised that mantle convection is driven by Earth's internal heat. However, whether or not chemical heterogeneities play an additional role in governing the style and vigour of convection remains debated (e.g. Christensen and Hofmann, 1994; Tackley, 1998; Davies, 1999; Davaille, 1999; Tackley, 2002; McNamara and Zhong, 2005; Tan and Gurnis, 2007; Bull et al., 2009; Schuberth et al., 2009b,a; Simmons et al., 2009, 2010; Schuberth et al., 2012).

Geochemical observations offer important insights into this debate, providing compelling evidence for compositional heterogeneity within the mantle. Most fundamentally, lavas sampled at the two main sites of mantle upwelling on Earth, mid-ocean ridge basalts (MORBs) and ocean–island basalts (OIBs), are chemically distinct. Their geochemical diversity has traditionally been attributed to the existence of large-scale mantle heterogeneity, in particular, to accessible reservoirs that differ in both depth and composition (e.g. Zindler and Hart, 1986; Allègre et al., 1996; Kellogg et al., 1999; Hofmann, 2003). However, reconciling geochemical constraints for isolated, yet accessible, mantle reservoirs, with

* Corresponding author.
E-mail address: Rhodri.Davies@imperial.ac.uk (D.R. Davies).

0012-821X/$ - see front matter © 2012 Elsevier B.V. All rights reserved.
http://dx.doi.org/10.1016/j.epsl.2012.08.016

geophysical observations of vigorous whole mantle convection remains a difficult task (e.g. Hager et al., 1985; Grand et al., 1997; van der Hilst et al., 1997; Helffrich and Wood, 2001; Tackley, 2002; van Keken et al., 2002; Davies, 2009). Recent debate has focused on the nature of large low-shear-velocity provinces (LLSVPs) in the deep mantle, beneath Africa and the Pacific. Do they represent long-lived, dense, chemically distinct reservoirs and, if so, to what extent do they influence mantle dynamics (e.g. Tackley, 1998, 2002; McNamara and Zhong, 2005; Deschamps and Tackley, 2008, 2009; Davies and Davies, 2009; Schuberth et al., 2009b,a; Simmons et al., 2009, 2010; Schuberth et al., 2012)?

Several seismic characteristics of LLSVPs may indicate that they are of a different bulk composition to surrounding mantle: (i) their shear wave velocity anomalies, which range from −2 to −4% in tomographic models (e.g. Houser et al., 2008; Ritsema et al., 2011) and are greater still in high-resolution regional travel-time studies (e.g. Wang and Wen, 2007) may be larger than expected for thermal heterogeneity alone (e.g. Karato and Karki, 2001; Brodholt et al., 2007); (ii) abrupt lateral transitions in shear wave velocity at the margins of these structures are generally considered too sharp for isochemical thermal features (e.g. Ritsema et al., 1998; Ni et al., 2002; To et al., 2005); (iii) observed lower mantle ratios between shear and compressional wave-speed anomalies are larger than mineral physics would predict for an isomorphic thermal structure (e.g. Karato and Karki, 2001; Saltzer et al., 2001; Brodholt et al., 2007); and (iv) anomalies in shear wave velocity, bulk-sound velocity and perhaps density, have been found to be of opposite sign (i.e. anticorrelated: Ishii and Tromp, 1999; Masters et al., 2000; Trampert et al., 2004; Simmons et al., 2010; Della Mora et al., 2011; Koelemeijer et al., 2012). Such observations suggest that LLSVPs are chemically anomalous. This interpretation has largely been supported by comparisons between seismic observations and synthetic mantle structures generated via numerical models of thermo-chemical convection, where chemically dense material focuses into large-scale structures beneath Africa and the Pacific (e.g. McNamara and Zhong, 2005; Bull et al., 2009). The scale of such structures would imply that chemical heterogeneity plays an important role in governing lower mantle dynamics.

However, other studies have questioned this conclusion, querying the extent of a chemical contribution to the seismic expression of LLSVPs (e.g. Schuberth et al., 2009b,a; Simmons et al., 2009; Malcolm and Trampert, 2011; Schuberth et al., 2012). Several independent lines of evidence imply that these regions are warmer (and more buoyant) than surrounding mantle: they underlie an elevated surface (Nyblade and Robinson, 1994; Gurnis et al., 2000), display large positive geoid anomalies (Hager et al., 1985) and exhibit extensive hot-spot volcanism (e.g. Duncan and Richards, 1991). In addition, they have not experienced significant subduction since the Jurassic. As a result, upwelling of hot buoyant mantle, fed from a thermal boundary layer at the core–mantle-boundary (CMB), would be expected to focus beneath Africa and the Pacific. Given a sufficient CMB heat flux, thermal heterogeneity could therefore provide a straightforward explanation for the distribution and amplitude of shear wave velocity anomalies in the deep mantle (Schuberth et al., 2009b,a). It has also been proposed that: (i) observed deep mantle anti-correlations between shear and bulk-sound velocity anomalies; and (ii) high ratios of shear to compressional wave-speed anomalies are largely a consequence of differential wave-front healing of shear and compressional waves, as opposed to chemical heterogeneity (Malcolm and Trampert, 2011; Schuberth et al., 2012). Furthermore, our ability to resolve lower mantle density heterogeneity is uncertain (Romanowicz, 2001) and, consequently, inferred anti-correlations between shear wave velocity and density anomalies must be treated with caution. When combined, such observations indicate that the seismic characteristics of LLSVPs could be dominated by thermal, as opposed to chemical, effects. Which scenario is most compatible with Earth's mantle—a system driven primarily by temperature variations or a system where chemical heterogeneity focuses into large-scale structures that modify the underlying dynamics—therefore, remains uncertain.

In this paper, we compare the forward modelled synthetic seismic velocity structures of isochemical and thermo-chemical 'pile' models, to determine which is most compatible with seismological observations of Earth's mantle. When examining such synthetic structures, previous studies have analysed the effects of 3-D spherical geometry, mantle compressibility, plate motion histories, thermodynamically self-consistent conversions of physical to seismic structure, anelasticity and limited seismic resolution (e.g. Tackley, 2002; McNamara and Zhong, 2005; Tan and Gurnis, 2007; Deschamps and Tackley, 2008, 2009; Schuberth et al., 2009b,a; Bull et al., 2009). However, their combined effects have not been evaluated in a consistent comparison between synthetic thermal and thermo-chemical structures and seismic observations, as we do here. Such a comparison is needed to quantify the relative importance of thermal and chemical heterogeneity in governing lower mantle dynamics and, in turn, generating lower mantle seismic heterogeneity.

2. Methods and models

2.1. Circulation models

We generate global temperature (T), pressure (P) and compositional (X) fields using a modified and benchmarked version of the spherical mantle convection code TERRA (Baumgardner, 1985; Bunge et al., 1997; Davies and Davies, 2009; Wolstencroft et al., 2009). Calculations are performed on a mesh with ~80 million discrete nodal points, thus providing the resolution necessary to explore mantle flow at Earth-like convective vigour (models achieve an internally heated Rayleigh number, based upon reference values, of $\mathrm{Ra}_H \approx 5\times10^8$, which is similar to estimates of the mantle's Rayleigh number). Our models incorporate compressibility, in the form of the anelastic liquid approximation, with radial reference values represented through a Murnaghan equation of state. Isothermal boundary conditions are prescribed at the surface (300 K) and CMB (4000 K), with the mantle also heated internally, at roughly chondritic rates (5.5×10^{-12} W kg^{-1}: for comparison, the heating rate in carbonaceous chondrites, often taken to be representative of mantle material, is 5.2×10^{-12} W kg^{-1}). A free-slip boundary condition is specified at the CMB, whilst surface velocities are assimilated according to 300 Myr of plate motion history (Stampfli and Borel, 2002; Stampfli and Hochard, 2009), at discrete 1 Myr intervals. Our extended plate motion history provides improved geographic and temporal constraints on mantle heterogeneity structure when compared to previous studies, where surface plate motions were imposed for a maximum of the past 120 Myr (e.g. Bunge et al., 1998; McNamara and Zhong, 2005; Schuberth et al., 2009b,a; Bull et al., 2009). Phase changes are incorporated at 410- and 660-km depth, with viscosity varying as a function of depth (z) and temperature (T), following the relation:

$$\mu(z,T)=\begin{cases}\mu_0\Delta\mu_{Li}\exp[V_a z'-E_a T'] & z<100\text{ km},\\ \mu_0\exp[V_a z'-E_a T'] & 100\text{ km}\le z<410\text{ km},\\ \mu_0\Delta\mu_{410}\exp[V_a z'-E_a T'] & 410\text{ km}\le z<660\text{ km},\\ \mu_0\Delta\mu_{660}\exp[V_a z'-E_a T'] & z\ge 660\text{ km},\end{cases} \quad (1)$$

where T' and z' are non-dimensionalised by ΔT and mantle depth, respectively, whilst V_a and E_a are non-dimensional constants

controlling the sensitivity of viscosity to depth and temperature. Our choice of V_a and E_a yields an Earth-like viscosity-depth profile, which results in model slab sinking rates that are consistent with those inferred from tomographic images. However, to ensure numerical stability, the temperature dependence of viscosity in our models is reduced when compared to current estimates for Earth's mantle (e.g. Ammann et al., 2009), with viscosity only decreasing by a factor of 100 over the temperature range ΔT. We note, however, that the imposed plate-motion conditions capture the influence of surface-plate strength and plate-boundary weakness on convective motions. For initial conditions, a standard convection model (with free-slip surface) is run until a thermal quasi-steady-state is achieved. Early Carboniferous mantle heterogeneity is then approximated by running models with global plate configurations fixed to the oldest available reconstruction at 300 Ma, for ≈ 50 Myr. The chemical field (X) is simulated via the ratio tracer particle method (Tackley and King, 2003; Stegman et al., 2003), with $\approx 2.0 \times 10^9$ active tracers, of two distinct types (dense material, $X=1$; regular material, $X=0$). Key model parameters are provided in Table 1, with radial profiles of density, thermal expansivity and viscosity in Supplementary Fig. 1.

From a whole suite of simulations, we focus on two cases: (i) a purely thermal model with no chemical heterogeneity; and (ii) a thermo-chemical 'pile' model, where chemically dense material focuses into distinct discontinuous structures at the mantle's base (e.g. Tackley, 1998, 2002; McNamara and Zhong, 2005). Whilst alternative conceptual thermo-chemical models have been proposed, such as metastable super-plumes (Tan and Gurnis, 2007) and thermo-chemical super-plumes (Davaille, 1999), all involve large volumes of concentrated dense material within broad upwelling regions, and all relate African and Pacific LLSVPs to large structures of intrinsically denser material (Bull et al., 2009). In our simulation, chemically anomalous material comprises only 3% of the mantle's volume, which is consistent with the volumetric predictions of Hernlund and Houser (2008). The model is initiated with a 175-km thick basal layer of excess density 2.75%, which progressively deforms as the model evolves. The buoyancy number, $B = \Delta\rho_X/\Delta\rho_T \approx 0.275$, where $\Delta\rho_T = \rho_s\alpha_s\Delta T_s$: ρ_s and α_s denote density and thermal expansion coefficient at the surface, respectively, whilst ΔT_s is the super-adiabatic temperature difference from surface to CMB. Our thermo-chemical model represents a scenario where pre-existing dense heterogeneity at the mantle's base is pushed around by the plate mode of mantle convection. However, models with both primitive and recycled heterogeneity can form similar deep mantle structures, whose size, stability and shape depend on the density and viscosity contrast between dense and background mantle material and are also strongly influenced by subduction history (e.g. Christensen and Hofmann, 1994; McNamara and Zhong, 2005; Tan and Gurnis, 2007; Deschamps and Tackley, 2008, 2009). To first order, our results are therefore also applicable to such recycling scenarios. Apart from the inclusion of dense material in the thermo-chemical model, both cases are identical. However, as we will show, their convective planforms and seismic expressions differ substantially, which allows for meaningful comparisons between each case and seismic observations of Earth's present day mantle.

Table 1
Parameters common to all models. Rayleigh numbers are calculated based upon surface reference values.

Parameter	Symbol	Value	Units
Surface temperature	T_s	300	K
CMB temperature	T_{cmb}	4000	K
Internal heating rate	H	5.5×10^{-12}	W kg^{-1}
Reference viscosity	μ_0	3.0×10^{21}	Pa s
Lithospheric multiplication-factor	$\Delta\mu_{Li}$	100	–
410-km multiplication-factor	$\Delta\mu_{410}$	5	–
660-km multiplication-factor	$\Delta\mu_{660}$	30	–
Viscosity: depth dependence	V_a	2.99	–
Viscosity: temperature dependence	E_a	4.61	–
Clapeyron slope: 410-km	Cl_{410}	1.5×10^6	M Pa K^{-1}
Clapeyron slope: 660-km	Cl_{660}	-1.0×10^6	M Pa K^{-1}
Surface density	ρ_s	3500	kg m^{-3}
CMB density	ρ_{cmb}	5568	kg m^{-3}
Surface thermal expansivity	α_s	3.8×10^{-5}	K^{-1}
CMB thermal expansivity	α_{cmb}	1.2×10^{-5}	K^{-1}
Superadiabatic temperature contrast	ΔT_s	2650	K
Total temperature contrast	ΔT	3700	K
Adiabatic footing temperature	T_{pot}	1600	K
Thermal conductivity	k	4.0	W m^{-1} K^{-1}
Specific heat capacity	C_p	1134	J kg^{-1} K^{-1}
Surface Dissipation number	Di_s	≈ 1.0	–
Volumetric Dissipation number	Di_V	≈ 0.5	–
Internally heated Rayleigh number	Ra_H	$\approx 5.0 \times 10^8$	–
Basally heated Rayleigh number	Ra_b	$\approx 3.0 \times 10^7$	–

2.2. Conversion from physical to seismic structure

Modelled (T,P,X) fields are converted into elastic parameters using lookup tables (pers. comm. Stixrude and Lithgow-Bertelloni, 2011), generated via a thermodynamic approach for a simplified model of mantle composition with six components: CaO, FeO, Na_2O, Al_2O_3, MgO and SiO_2 (for further details see Stixrude and Lithgow-Bertelloni, 2005, 2011). This approach naturally accounts for the sensitivity of seismic velocities to pressure, temperature, composition and phase, inclusive of the post-perovskite phase at lowermost mantle depths (e.g. Sidorin et al., 1999; Oganov and Ono, 2004; Murakami et al., 2004).

For the frequency range of seismological observations, elastic velocities must be corrected for the effects of temperature- and pressure-dependent anelasticity (e.g. Karato, 1993). Such a correction increases the non-linear sensitivity of seismic velocities to temperature (Fig. 1d–f). It is achieved here using anelasticity model Q4, which is constrained by seismological models of attenuation and laboratory measurements (Goes et al., 2004). Within the range of plausible anelastic mantle parameters (e.g. Matas and Bukowinski, 2007; Brodholt et al., 2007), Q4 is an end-member with a relatively low temperature sensitivity. For comparison, Fig. 1f illustrates model Q6, which has a more average temperature sensitivity (Goes et al., 2004; Cobden et al., 2009).

For the purely thermal case, we assume a pyrolitic composition in our conversion of modelled (T,P,X) to seismic velocity. We also assume a pyrolitic composition for background mantle in the thermo-chemical case. However, for the dense chemical component, two seismic scenarios are considered, with either a basaltic (representative of recycled dense subducted material) or an iron-rich (as a potential dense primitive material) composition assumed (Table 2). The thermodynamic compilation used (Stixrude and Lithgow-Bertelloni, 2011) predicts that outside of the post-perovskite stability field, basaltic material is significantly faster in shear wave velocity and slightly faster in compressional wave velocity, when compared to a pyrolite (Fig. 1a,c). Conversely, the iron-rich composition is substantially slower in both shear and compressional wave velocities. Under lower mantle conditions, both materials have similar excess densities, relative to pyrolite (Fig. 1b). As a consequence, both synthetic seismic scenarios can be generated from the same underlying dynamical model. Note that other melt-depleted, peridotitic or chondritic compositions have similar velocities to pyrolite, with differences only in detailed phase transition structure (Cobden et al., 2009) and, hence, are not considered here.

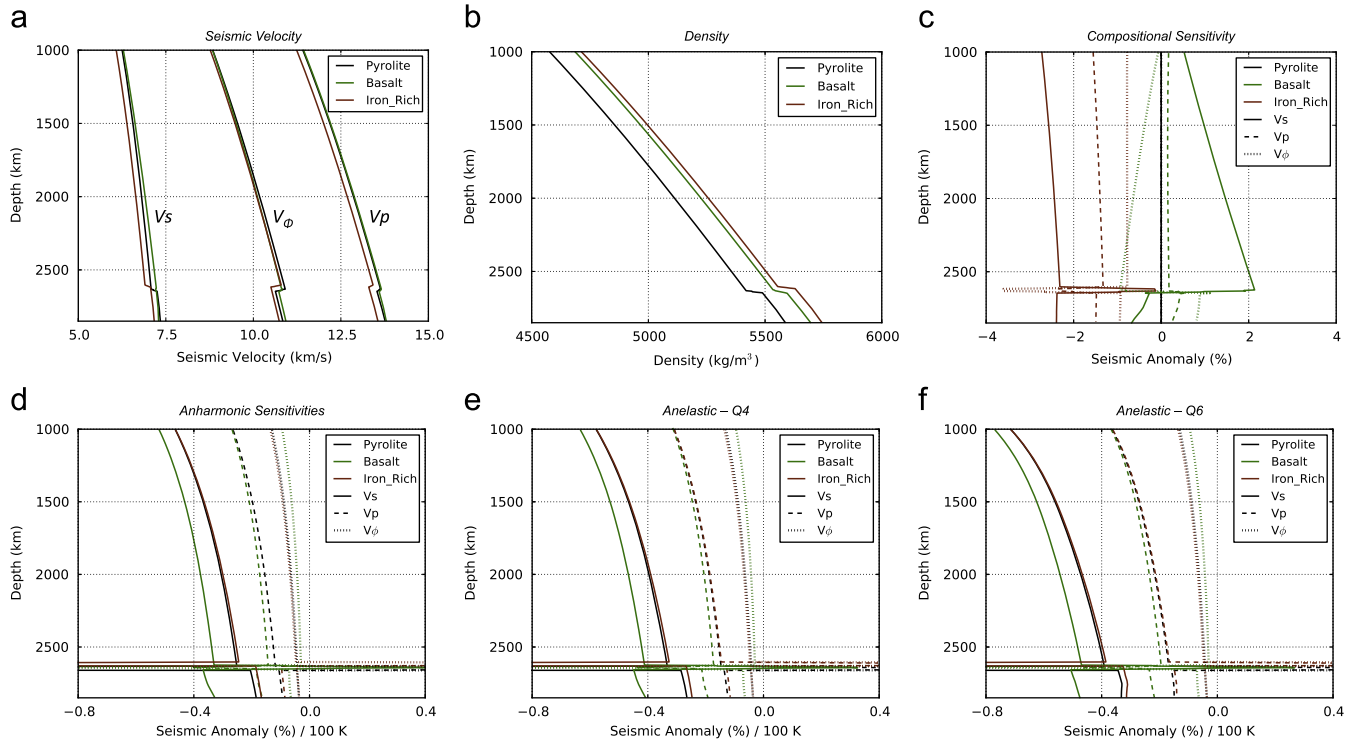

Fig. 1. (a) Seismic velocities, V_P, V_S, V_ϕ and (b) density, along an adiabat with a potential temperature of 1573 K, for all compositions examined in this study (Stixrude and Lithgow-Bertelloni, 2011); (c) compositional derivatives of seismic velocity compared to a pyrolitic reference; (d) temperature derivatives of elastic velocities—the horizontal axis shows the percent change per 100 K temperature increase from an adiabat with a potential temperature of 1573 K; (e) as in (d), but corrected for the effects of temperature dependent anelasticity using model Q4, an end-member anelasticity model with relatively low temperature sensitivity (Goes et al., 2004); (f) as in (d), but corrected using anelasticity model Q6, which has an intermediate temperature sensitivity (Goes et al., 2004). Note that all results presented in this paper utilise model Q4 when correcting for anelastic effects—the temperature sensitivity of model Q6 is illustrated for comparison only.

Table 2
Major-oxide compositions (in mol%) examined in this study.

Component	Pyrolite	Basaltic	Fe-rich
SiO_2	38.71	51.57	40.03
MgO	49.85	14.94	43.37
FeO	6.17	7.06	11.68
CaO	2.94	13.88	3.24
Al_2O_3	2.22	10.19	1.68
Na_2O	0.11	2.18	0.0

In our comparisons with seismic observations, we present the raw synthetic velocity structures (i.e. those resulting directly from conversion between model (T, P, X) fields and seismic velocity), in addition to structures that have been filtered for the effects of tomographic imaging, using the resolution operator of the shear wave tomography model S40RTS (Ritsema et al., 2011). Tomographic resolution is limited by uneven geographic data coverage, model parametrization and the damping and smoothing applied in the tomographic inversion: the resolution filter captures these effects (Ritsema et al., 2007, 2011). Different global tomographic models generally agree on the large-scale structure of Earth's lower mantle, but recover different anomaly amplitudes and relative strengths of shear and compressional velocity heterogeneity (e.g. Becker and Boschi, 2002). Differing model resolution is likely a large contributor to such discrepancies and, hence, comparisons between model predictions and tomography without application of such a resolution operator can be misleading (e.g. Mégnin et al., 1997; Davies and Bunge, 2001; Ritsema et al., 2007; Bull et al., 2009; Schuberth et al., 2009a). As resolution filters for other tomographic models are not yet available, we focus our quantitative comparison with tomography solely on S40RTS. For other seismic constraints, we can, at this time, only compare the unfiltered, 'full resolution', synthetic structures with imaged velocities.

3. Results

Present-day snapshots of the thermal and compositional fields from our simulations are presented in Fig. 2. In both cases, the upper mantle planform is dominated by strong downwellings in regions of present-day plate convergence. In the mid-mantle, cold downwellings are prominent beneath North America (the subducted Farallon slab) and South-East Asia (the former Neo-Tethys ocean, Fig. 2a), whilst remnants of older subduction are visible above the CMB (Fig. 2c/f). These downwellings modulate the location of hot material such that it becomes concentrated into large-scale structures beneath Africa and the Pacific (Fig. 2b/e), with the majority of plumes rising from their margins, in both cases, which is consistent with observations (e.g. Thorne et al., 2004; Burke et al., 2008). The Pacific anomaly is reasonably circular, whilst the African anomaly is a NW-SE trending structure, which to the north curves eastward under Europe and to the south extends into the Indian Ocean. In the purely thermal case, these structures comprise clusters of plumes and interconnected hot, linear ridges, whilst they represent discontinuous chemical 'piles', which cover around 50% of the CMB, in the thermo-chemical case (Fig. 2d). Note that similar distributions of heterogeneity are observed in models that assimilate only 120 Myr of plate motion history (e.g. McNamara and Zhong, 2005). However, the extended subduction history and improved geographic constraints incorporated herein lead to more

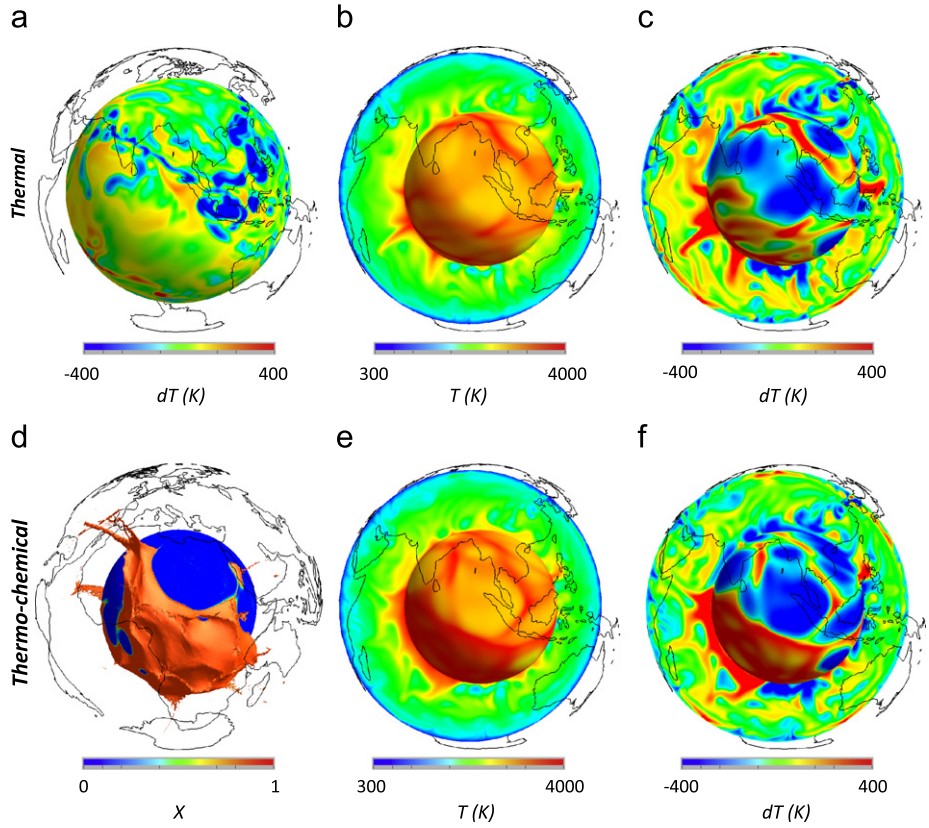

Fig. 2. (a) The temperature field, away from the layer average (i.e. the thermal anomaly), at 1200-km depth, for the purely thermal case. The view is centred on the Indian Ocean (continental boundaries provide geographic reference), illustrating subducted remnants of the former Tethys Ocean; (b)/(c) snapshots of the absolute temperature and temperature anomaly fields, respectively—images include a radial surface at 2800-km depth and a cross-section highlighting the thermal structure beneath Africa; (d) the chemical interface beneath Africa, from our thermo-chemical 'pile' model, mapped by the $X=0.9$ iso-surface, which overlies a radial surface at 2800-km depth; (e)/(f) analogous to (b)/(c), but illustrating the convective planform for the thermo-chemical 'pile' model.

concentrated structures in the deep mantle beneath Africa and the Pacific than previously predicted.

3.1. Distribution of thermal and chemical heterogeneity

Histograms displaying the thermal heterogeneity structure for each case are presented in Fig. 3. Focussing initially on the purely thermal case, we observe that the temperature distribution is dominated by thermal boundary layers at the surface and CMB (Fig. 3a). The layer average temperature is slightly sub-adiabatic in the lowermost mantle, as expected for an isochemical convecting system with substantial internal heating (e.g. Jeanloz and Morris, 1987; Parmentier et al., 1994; Bunge, 2005). The temperature anomaly histogram for this case (Fig. 3b) illustrates that the majority of model grid points have temperatures at, or near to, the mean radial value, owing to the high convective vigour of the simulation. Nonetheless, substantial temperature anomalies exist, with maximum cold thermal anomalies (slabs) on the order of 1000–1300 K, at all depth levels (minor fluctuations with depth can be related to variations in the amount of subducted material at different stages of the plate motion history). We observe large plume excess temperatures (maximum hot thermal anomalies—Fig. 3b) of around 1300 K in the lower mantle, which reduce to 300-400 K in the upper mantle, consistent with petrological estimates of plume excess temperatures (e.g. Schilling, 1991; Herzberg et al., 2007). This strong decrease in plume excess temperature towards the surface is a consequence of plumes rising adiabatically in the otherwise sub-adiabatic mantle (see Bunge, 2005; Leng and Zhong, 2008, for detailed discussion).

In the thermo-chemical case, the excess density of chemical 'piles' acts to prevent the advection of material away from these regions. Although there is convection within the 'piles', which homogenises most internal structure, heat can only conduct across the chemical interface. Consequently, 'piles' heat up substantially when compared to background mantle and the boundary layer thickens in comparison to the purely thermal case (cf. the relative positions of $\log_{10}(\mathrm{NGP})=3$ and $\log_{10}(\mathrm{NGP})=4$ contours in the lowermost mantle between Fig. 3a and d). Although dense material is predominantly restricted to the mantle's lowermost 700-km (Fig. 3f), plumes rising from the chemical interface carry elevated temperatures up to 1200-km above the CMB (cf. dashed lines of thermal and thermo-chemical cases in Fig. 3c). These hot regions increase the average geotherm, such that it becomes super-adiabatic in the lowermost mantle. As a result: (i) lower mantle cold thermal anomalies are generally increased relative to the purely thermal case (note the relative positions of $\log_{10}(\mathrm{NGP})=3$ and $\log_{10}(\mathrm{NGP})=4$ contours in the lowermost mantle between Fig. 3b and e); and (ii) most model grid points display strong negative (slabs) or positive ('piles') temperature anomalies in the lowermost mantle, which differs to the purely thermal case, where the majority of model grid points have temperatures at, or near to, the mean radial value (cf. $\log_{10}(\mathrm{NGP})=4$ contours in the deep mantle between Fig. 3b and e). Chemical 'piles' also influence the CMB heat flux: the present-day CMB heat flux decreases from ~ 10 TW in the purely thermal case, to ~ 7 TW in the thermo-chemical case. It is clear therefore that including even a small volume-fraction of concentrated dense chemical heterogeneity has a significant influence on the thermal

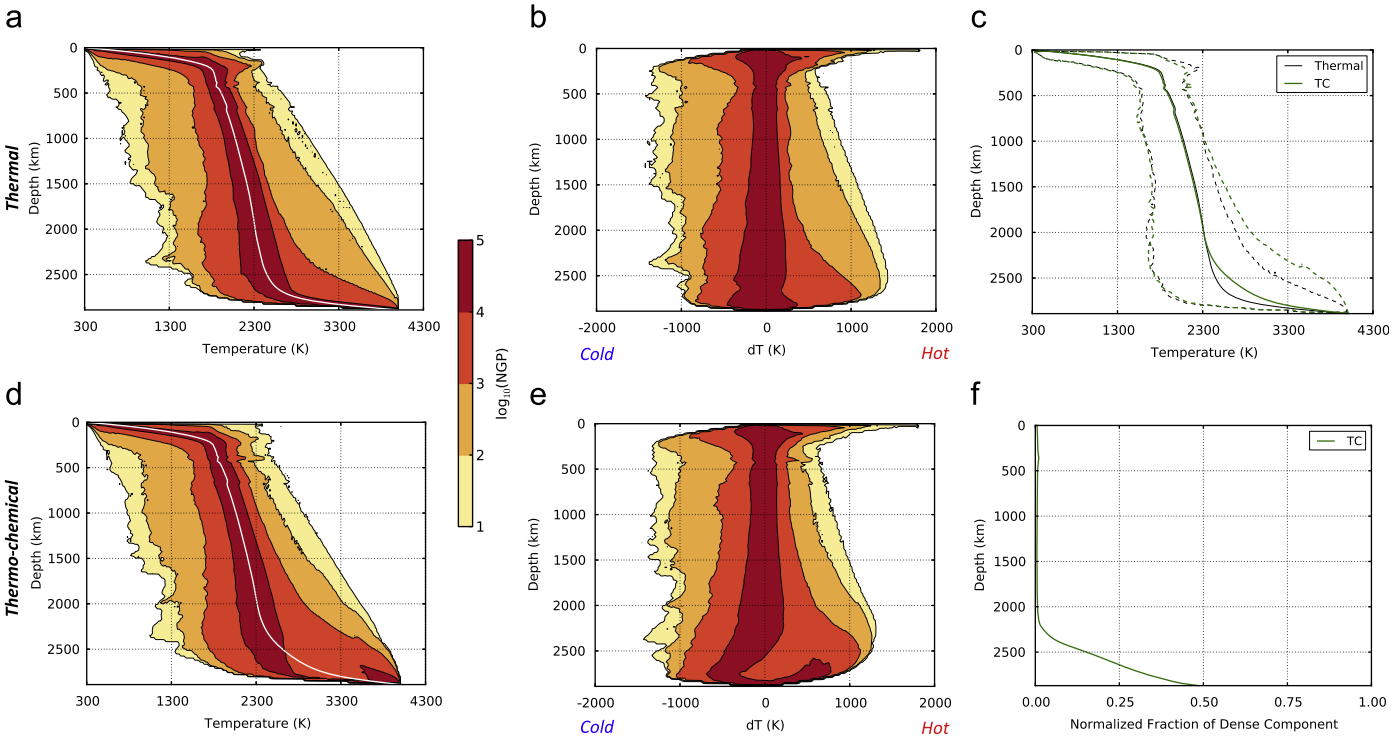

Fig. 3. Histograms displaying: (a)/(d) the temperature distribution; and (b)/(e) the distribution of temperature anomalies, relative to the radial average, as a function of depth, for the purely thermal and thermo-chemical 'pile' models examined herein. The logarithmic colour scale and contours represent the total number of model grid points (NGP) at any given depth (vertical axes). Continuous white lines denote radially averaged temperature profiles, which are compared in subfigure (c), where dashed lines, outlining the $\log_{10}(\mathrm{NGP})=3$ contour, provide an insight into the dominant range of temperatures at any given depth, thus allowing for a simple comparison between both cases; (f) the volume fraction of dense material at any given depth in the thermo-chemical 'pile' case.

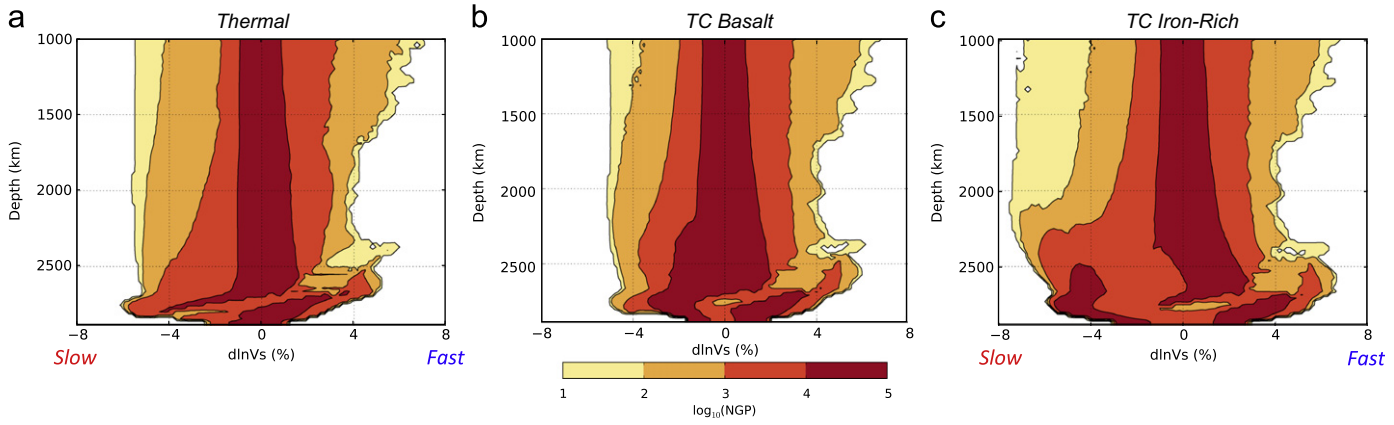

Fig. 4. Histograms displaying lower-mantle shear wave velocity anomalies as a function of depth. The logarithmic colour scale and contours represent the total number of model grid points (NGP) at any given depth. For the thermo-chemical case, dense material is converted into seismic velocity assuming either a basaltic (TC Basalt) or iron-rich (TC Iron-Rich) composition (see text for details), whilst a pyrolitic composition is assumed for ambient mantle and the purely thermal case. Note that anomalies are calculated from the layer average shear wave velocity.

heterogeneity structure. This, in turn, has a considerable effect on the distribution of shear wave heterogeneity.

3.2. Distribution of shear-wave heterogeneity

Histograms of lower mantle shear wave velocity anomalies are presented in Fig. 4. There are clear differences between each case and they display little resemblance to their associated thermal structures. Focussing first on the purely thermal case (Fig. 4a), we observe that maximum fast anomalies decrease strongly as a function of depth, even though corresponding maximum cold temperature anomalies remain fairly constant (Fig. 3b). In addition, maximum slow anomalies are reasonably consistent with depth, despite plume excess temperatures increasing. These trends are to be expected, since the sensitivity of seismic velocity to temperature decreases strongly with increasing pressure (Fig. 1d–f). The shear wave velocity distribution also shows an asymmetry between maximum slow and fast seismic anomalies below 1500-km depth, with negative anomalies being generally larger than their positive counterparts. This arises from the non-linear sensitivity of seismic velocity to absolute temperature (positive temperature anomalies produce larger shear wave velocity variations than negative anomalies), due to anelastic effects (e.g. Karato, 1993; Goes et al., 2004). The observed lowermost mantle discontinuity below ~2500-km depth and the general increase in heterogeneity is a consequence of topography on the strongly exothermic phase transition from perovskite to post-perovskite

(pv-ppv: Nakagawa and Tackley, 2006), which produces a sharp increase in shear wave velocity (Fig. 1a). However, an increase in lowermost mantle seismic heterogeneity would be expected, and is indeed observed, in the absence of this phase transition, due to increased thermal heterogeneity at these depths (Fig. 3b).

In both thermo-chemical cases (Fig. 4b and c), lowermost mantle fast seismic anomalies increase relative to the purely thermal case, due to the stronger negative temperature anomalies observed at these depths, as described in Section 3.1. A distinct region of slower than average velocities is also evident, extending several hundred kilometres above the CMB, which corresponds to the seismic expression of hot 'pile' material (cf. relative positions of $\log_{10}(\mathrm{NGP})=4$ shear wave anomaly contours in the lowermost mantle between thermal and thermo-chemical models). For basalt, which is generally faster in shear wave velocity than a pyrolite at lower mantle depths (Fig. 1c), the chemical effect on seismic velocity counteracts the effect of increased temperature and, accordingly, the range of seismic anomalies in the basaltic case is similar to that displayed in the purely thermal case. However, for iron-rich material, which is slower than pyrolite at lower mantle depths (Fig. 1c), thermal and chemical effects combine to produce 'piles' with substantially stronger negative shear wave anomalies. Such strong anomalies also bias the one-dimensional seismic average and, as a result, the range of anomalies increases in comparison to other cases.

3.3. Amplitude of imaged heterogeneity structure

The strongest LLSVP anomaly amplitudes are inferred from regional waveform and travel-time modelling studies. For example, Ni and Helmburger (2003), Wang and Wen (2007) and He and Wen (2009) infer that African and Pacific LLSVPs have a shear wave velocity structure with average velocity perturbations of -5% at the base and -2% to -3% in the mid-lower mantle. Even with the minimum temperature-dependence of anelasticity model Q4 used herein, all models examined produce such large amplitude low-velocity anomalies and a strong increase in heterogeneity towards the mantle's base (Fig. 4).

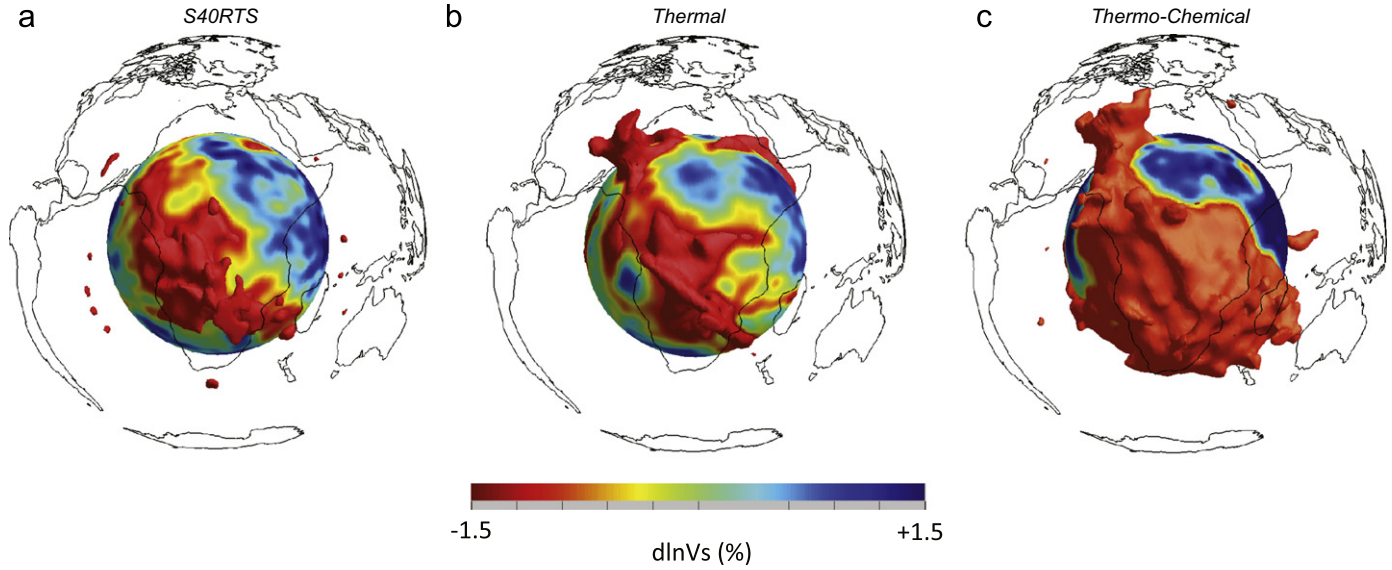

Fig. 5. Shear wave velocity perturbations beneath Africa from: (a) tomographic model S40RTS; (b) our purely-thermal model; and (c) our thermo-chemical model, where the dense chemical component represents only 3% of the mantle volume. In the isochemical model, (T,P,X) is converted into seismic velocity assuming a pyrolitic composition, whilst the thermo-chemical model illustrated here assumes a pyrolitic composition for background mantle and an iron-rich composition for the dense chemical component. The structure of a thermo-chemical model with a basaltic dense component has similar characteristics. We account for the geographic bias, smearing and damping inherent to tomographic models using the resolution operator of S40RTS (Ritsema et al., 2011, 2007), thus allowing for direct comparison between our models and S40RTS. All images include a radial surface at 2850-km depth and an isosurface at -1.0%, clipped above 1400-km to allow visualisation of lower mantle features. Continental boundaries are included for geographic reference.

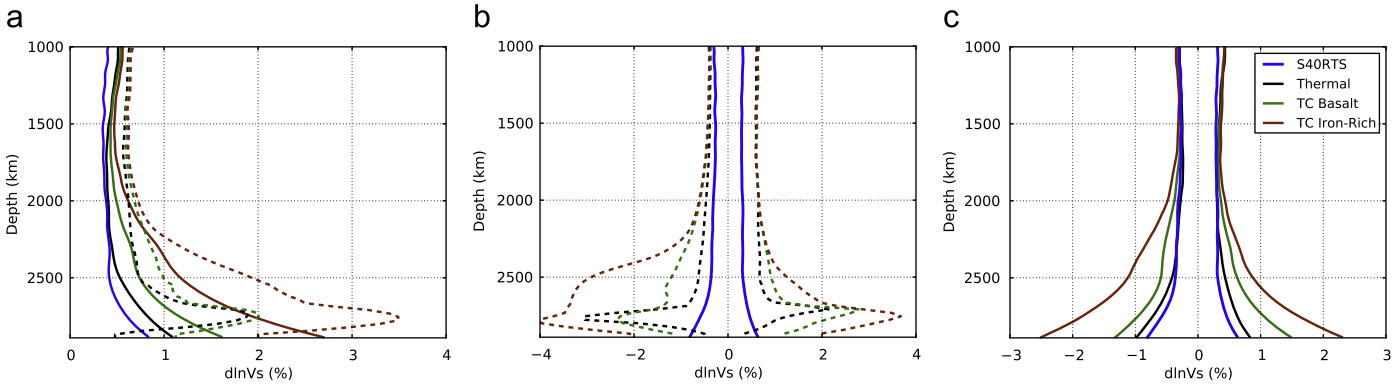

Fig. 6. (a) RMS amplitudes of shear wave velocity anomalies as a function of depth, for all cases examined, compared to tomographic model S40RTS. Dashed and continuous lines represent the RMS amplitudes before and after accounting for the effects of limited seismic resolution, respectively. Contributions are also decomposed into positive and negative components: (b) before and (c) after application of the resolution operator.

To better determine which scenario is most compatible with the imaged structure of Earth's mantle, the imaging method's limited resolving power must be accounted for. In Fig. 5, we compare the shear wave velocity distribution beneath Africa, from each case, to the tomographic model S40RTS (Ritsema et al., 2011) after 'filtering' our model output to account for the geographic bias, smearing and damping inherent to the tomographic inversion (Ritsema et al., 2007). Accordingly, our models and S40RTS are directly comparable in this figure. Although discrepancies are to be expected, the purely thermal case displays many similarities to S40RTS: the general character, geographic distribution and morphology of seismic anomalies are in close agreement. Thermo-chemical 'pile' cases, by contrast, exhibit large-scale and large-amplitude heterogeneity, which differs from the tomographic model.

Depth averaged RMS amplitudes of shear wave velocity heterogeneity, before and after seismic 'filtering', are compared in Fig. 6, with contributions also decomposed into positive and negative components. Application of S40RTS' resolution operator reduces the amplitudes of heterogeneity in all cases, especially in the lowermost mantle, where the RMS peak resulting from topography on the pv-ppv phase transition, visible in the unfiltered profiles, is lost. After 'filtering', the purely thermal model's RMS profile corresponds well to that of S40RTS, with heterogeneity almost constant at values of $\sim 0.4\%$ across most of the lower mantle and increasing strongly within ~ 400-km of the CMB, reaching values close to 1% (Fig. 6a). Furthermore, the lower mantle skew observed in S40RTS, and also found in other tomographic models (Hernlund and Houser, 2008), where negative values are greater than equivalent positive values, is reproduced (Fig. 6c).

For thermo-chemical models, regardless of whether 'piles' are of basaltic or iron-rich composition, RMS amplitudes of lowermost mantle heterogeneity are substantially greater than both the purely thermal case and S40RTS (factors of ≈ 2 and ≈ 3.5 larger than S40RTS, for basaltic and iron-rich models, respectively). This is a consequence of: (i) the distribution of thermal and chemical heterogeneity being such that the amplitude of lowermost mantle seismic anomalies are increased in the unfiltered data—as highlighted in Section 3.2, this is particularly true for the iron-rich case; and (ii) the presence of larger-scale structures, which are better recovered by tomographic inversion (cf. convective planforms of thermal and thermo-chemical cases in Fig. 2c/f). In thermo-chemical cases, heterogeneity also begins to increase from around 1200-km above the CMB, due to the presence of plumes rising from the interface between chemical 'piles' and background mantle (see Fig. 3c). This is different to S40RTS, where heterogeneity only begins to increase within ~ 400-km of the CMB. Note that if 'piles' are of basaltic composition, the lower mantle skew towards negative anomalies is not reproduced.

It is important to note that other tomographic models also display an increase in heterogeneity below 2200–2500-km depth, which is consistent with S40RTS (e.g. Becker and Boschi, 2002; Hernlund and Houser, 2008). Furthermore, although the anomaly amplitudes of S40RTS are lower than most other tomographic models (cf. Becker and Boschi, 2002), the low velocity amplitudes of all tomographic models are less than those of our unfiltered synthetic structures. It is interesting to note that with different inversion parameters, S40RTS can recover anomalies of a similar amplitude to other tomographic models (Ritsema et al., 2011), suggesting that the tomographic variability may, in large part, be due to differences in the data, parameterizations and inversion parameters of individual tomographic models. However, this can only be tested once resolution operators for other models become available.

3.4. Shear-wave velocity gradients

To investigate the abruptness of lateral shear wave velocity variations in our models we directly examine unfiltered structure, as sharp sides have been inferred from rapid travel-time variations and waveform complexity, rather than tomographic studies (e.g. Ritsema et al., 1998; Ni et al., 2002; To et al., 2005). Although sharp gradients in seismic velocity are often advanced as an argument in favour of chemical variations, strong lateral gradients are produced in all cases examined (Fig. 7). In the lowermost mantle (below 2000-km depth) of our purely thermal case, hot thermal anomalies beneath Africa and the Pacific are closely bounded by cold material (Fig. 2c), generating large thermal gradients of 800–1000 K/100 km. Such thermal gradients equate to shear wave velocity gradients of 3.5–4.5% per 100 km, which are within the range of 1.3–6% per 100 km observed seismically (lower bound—To et al., 2005; upper bound—Ni et al., 2002). This would suggest that chemical heterogeneity need not be invoked to explain the high seismic velocity gradients observed in the deep mantle beneath Africa and the Pacific. Note that gradients are further increased, in all cases, if one corrects for anelastic effects using model Q6, as opposed to Q4, due to its increased sensitivity to temperature (cf. Fig. 1e and f).

As chemical diffusion is negligible, the chemical interface between dense material and background mantle is very sharp in our thermo-chemical 'pile' cases (Fig. 2d). This produces temperature gradients of 950–1200 K/100 km (Fig. 2f), which are greater than those of our purely thermal case. Nonetheless,

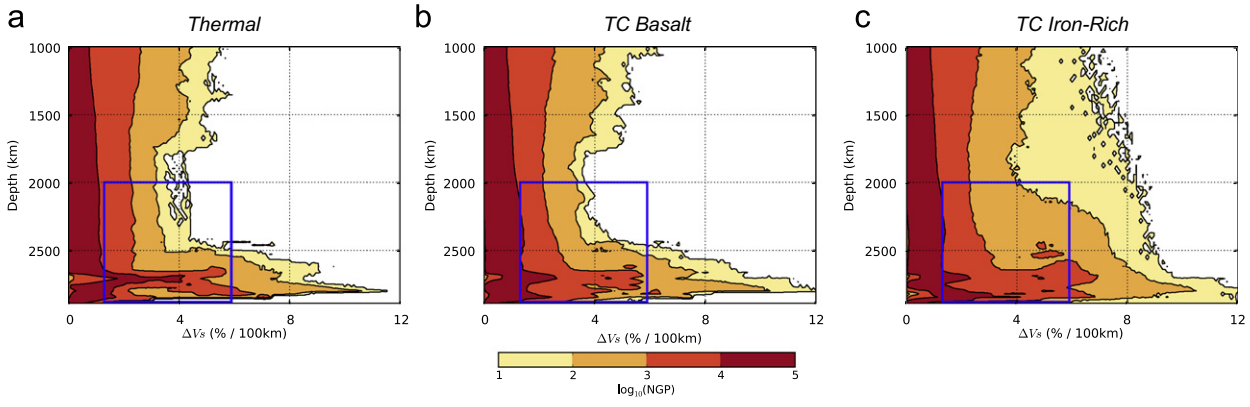

Fig. 7. The distribution of shear wave velocity gradients (% change per 100 km) as a function of depth, for all cases examined. Seismic constraints fall within the blue box, with the lower bound derived from the study of To et al. (2005) and the upper bound from Ni et al. (2002). (For interpretation of the references to color in this figure caption, the reader is referred to the web version of this article.)

similar shear wave velocity gradients are observed in the basaltic thermo-chemical case to the purely thermal case, as the chemical effect on shear wave velocity partially counteracts the thermal effect. However, larger gradients are observed in the iron-rich case, as chemical and thermal effects on shear wave velocity combine. In all cases, the lower mantle pv-ppv phase transformation causes a sharp increase in shear wave velocity (e.g. Wookey et al., 2005; Ammann et al., 2010; Stixrude and Lithgow-Bertelloni, 2011) and topography on this phase boundary produces local velocity gradients of greater than 10% per 100 km (Stixrude and Lithgow-Bertelloni, 2007). Such large lateral gradients are sufficient to explain sharp seismic reflections observed within the Pacific LLSVP (Lay et al., 2006).

It is important to note that the geographical location of high shear wave velocity gradient regions is somewhat different between purely thermal and thermo-chemical 'pile' models. In our thermo-chemical models, very little heterogeneity occurs within the 'piles', as is clear from Fig. 2 (also Fig. 9, which we discuss later) and, consequently, high shear velocity gradients are primarily restricted to 'pile' margins. By contrast, in the purely thermal model, the unfiltered shear-velocity heterogeneity structure beneath Africa and the Pacific is more intricate, being generated by plumes and interconnected hot, linear ridges. Accordingly, high shear wave velocity gradients do not only occur at the margins of these structures, but also within their interiors. Whilst current seismic studies support the notion that LLSVPs have high shear wave velocity gradients at their margins (e.g. Ni et al., 2002; To et al., 2005; Garnero et al., 2007), their interiors have not yet been probed in sufficient detail to determine whether or not internal structure exists. Nonetheless, there is some evidence for clusters and ridge-like structures that may be similar to those predicted in our purely thermal case (e.g. Ni and Helmburger, 2003; He and Wen, 2009).

3.5. The seismic ratio: $R = \mathrm{d}\ ln\ V_S / \mathrm{d}\ ln\ V_P$

Observed lower mantle ratios between shear and compressional wave-speed anomalies, $R = \mathrm{d}\ ln\ V_S / \mathrm{d}\ ln\ V_P$, are often cited as firm evidence for compositional heterogeneity at depth (e.g. Masters et al., 2000; Karato and Karki, 2001; Saltzer et al., 2001; Tan and Gurnis, 2007). Theoretically, ratios between different wave speeds are an excellent diagnostic for quantifying the relative contributions of thermal and chemical heterogeneity to seismic velocities. However ratio measurements are strongly influenced by (different) uncertainties in shear and compressional wave speed anomalies and their one-dimensional reference profiles (e.g. Karato and Karki, 2001; Ritsema and van Heijst, 2002; Cammarano et al., 2003; Brodholt et al., 2007; Cobden et al., 2009; Della Mora et al., 2011).

Histograms displaying lower mantle distributions of R are presented in Fig. 8a–c. Above $\sim$2200-km depth, these are similar for all cases: the majority of model grid points have R values of $\sim$2, although a substantial range is predicted, with extreme

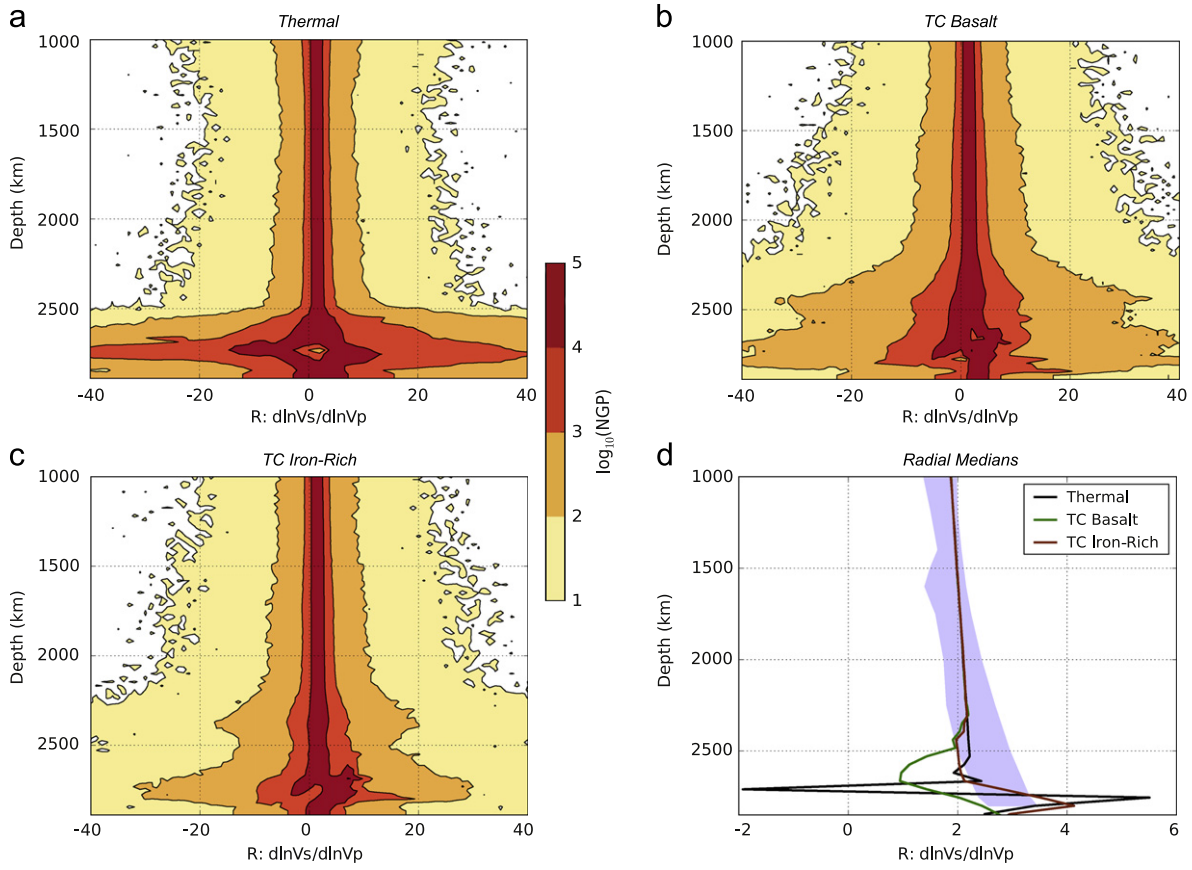

Fig. 8. (a)–(c) Histograms displaying lower mantle distributions of the seismic ratio, calculated via $R = \mathrm{d}\ ln\ V_S / \mathrm{d}\ ln\ V_P$, for all models; (d) R as a function of depth, compared to seismological observations (shaded blue region: Robertson and Woodhouse, 1995; Su and Dziewonski, 1997; Kennett et al., 1998; Masters et al., 2000; Saltzer et al., 2001; Karato and Karki, 2001; Ritsema and van Heijst, 2002). For (d), R is calculated by taking the ratio of all grid nodes with non-zero values of both compressional and shear wave velocity perturbations. A histogram of these nodal values is made and the median value chosen at each depth (following Masters et al., 2000). Unlike mean values, medians are not biased by relatively local regions with extreme values of R. Note that our models have not been post-processed to account for the limited resolution and non-uniqueness inherent to the seismic data and, hence, models and data are not directly comparable.

values of $\sim \pm 20$ occurring where compressional wave velocity anomalies approach zero. Below $\sim$2200-km depth, the range of R values increases dramatically, with the distribution becoming less systematic around the mean. It is at these depths that models differ: in the purely thermal case, the increased range results from lateral variations in depth of the post-perovskite phase transition. Relative to perovskite, post-perovskite has an increased shear wave velocity, a decreased compressional wave velocity and, hence, higher R (e.g. Wookey et al., 2005; Ammann et al., 2010; Stixrude and Lithgow-Bertelloni, 2011). Material that has transformed into post-perovskite also biases one-dimensional radial averages, such that strong negative values of R are observed in material that has not yet transformed (Stixrude and Lithgow-Bertelloni, 2007; Styles et al., 2011). The increased range of R values in the lowermost mantle of our thermo-chemical cases is caused by the pv-ppv phase transition, combined with the presence of anomalous chemical 'piles'.

Fig. 8d shows the median value of R, as a function of depth, for all cases, alongside seismological estimates, which require R to increase with depth, from 1.4–2.0 at 1000-km depth to 2.6–3.4 above the CMB (e.g. Robertson and Woodhouse, 1995; Su and Dziewonski, 1997; Kennett et al., 1998; Masters et al., 2000; Saltzer et al., 2001; Karato and Karki, 2001; Ritsema and van Heijst, 2002; Della Mora et al., 2011). Although imaged seismic structure shows a gradual increase in R as a function of depth, all models show rapid changes in the lowermost mantle. Such rapid variations would not be resolved by seismic methods (e.g. Della Mora et al., 2011). Indeed, it is important to note that models and seismic data are not directly comparable in this figure, as models have not been filtered to account for limited seismic resolution. Nonetheless, interesting trends are observed.

Above 2200-km depth and consistent with the histograms described previously, all our model ratios are similar, falling within the bounds of seismic observations. Below this depth however, R differs between each case. In the basaltic thermo-chemical case, lowermost mantle R values fall below the seismological bounds, dropping to $\sim$1 at 2600-km depth. Here, the dominant seismic anomalies are of a hot basalt relative to pyrolitic background mantle. Compared to pyrolitic material, basalt is significantly faster in shear wave velocity but only slightly faster in compressional wave velocity (Fig. 1c). Accordingly, in basaltic 'piles', the high temperature effect on shear wave velocity is partially offset by the compositional effect, but the high temperature effect on compressional wave velocity is only mildly affected. As a consequence, shear and compressional wave velocity anomalies are more similar than would be the case in the

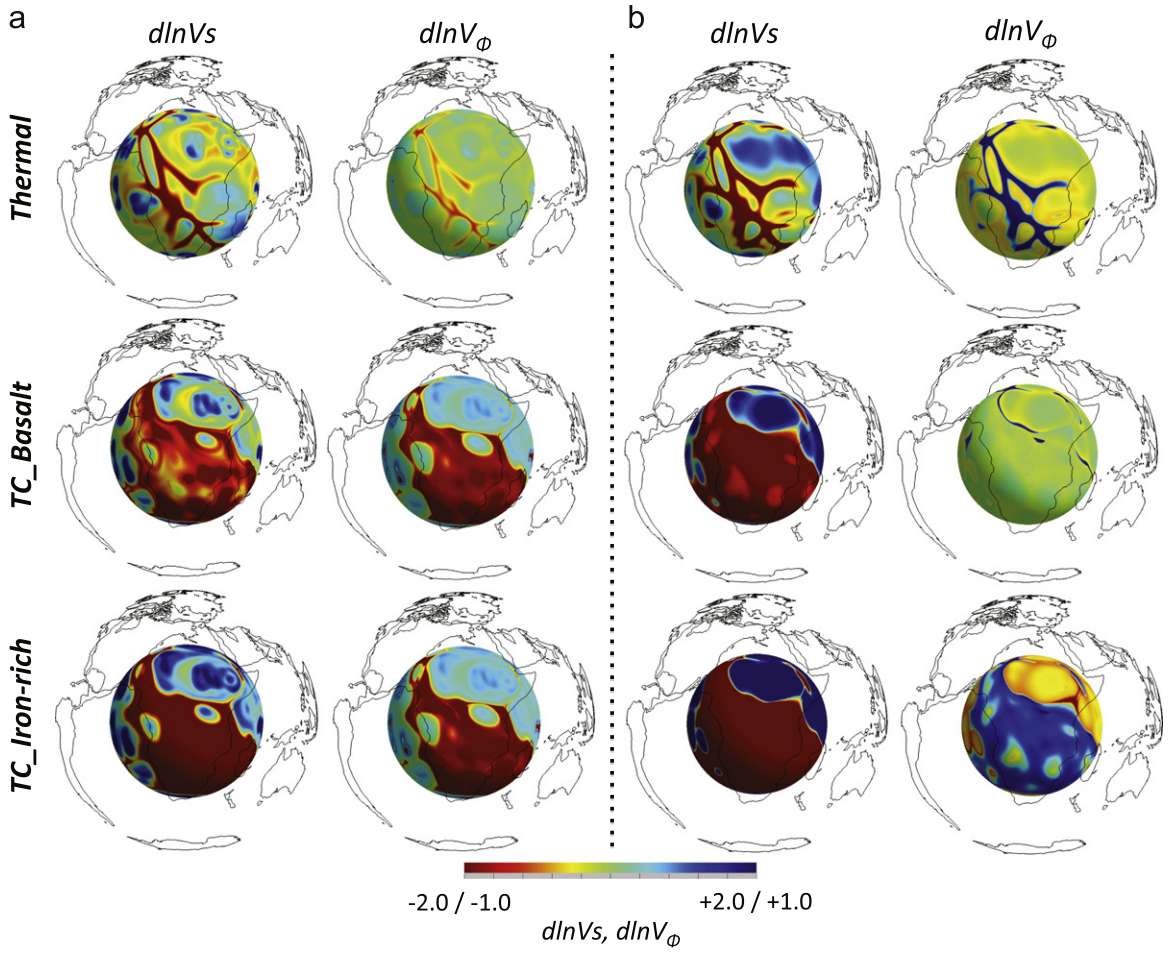

Fig. 9. Unfiltered shear wave (d $ln\ V_S$) and bulk-sound (d $ln\ V_\phi$) velocity anomalies beneath Africa for the models examined herein. Images include a radial surface at: (a) 2500-km; or (b) 2800-km depth. At 2500 km, shear and bulk-sound velocity anomalies are well correlated in all models. However, at 2800 km, both purely thermal and iron-rich thermo-chemical models display a strong anti-correlation, with bulk-sound velocity anomalies increasing as shear wave velocity anomalies decrease. This anti-correlation occurs in regions that have transformed to post-perovskite. In basaltic material, the post-perovskite phase transition has a less dramatic effect on seismic properties and, accordingly, only a weak anti-correlation is observed at 2800-km depth in this model (note that slithers of strong anti-correlation occur in background pyrolitic mantle). It is important to note that seismology would not see these anomalies as they are displayed here. They would be smoothed and distorted in a similar way to what is seen after application of S40RTS' resolution filter in Fig. 5, but with different resolution for V_S and V_ϕ anomalies. This would reduce the morphological differences observed between thermal and thermo-chemical cases.

absence of chemical heterogeneity, resulting in the decreased ratios observed. As one approaches the CMB, greater volume-fractions of material become basaltic (Fig. 3f) and thermal effects begin to dominate R once again, with the ratio increasing. Furthermore, at these depths, both basaltic and pyrolitic material transforms into post-perovskite, which has a higher R than its perovskite counterpart.

The iron-rich case, by contrast, generally exhibits increased ratios in the lowermost mantle: unlike basaltic material, the high temperature effect on R is enhanced by seismically slow iron-rich compositions. For the purely thermal case, values within, above and below seismological observations are predicted, with R increasing to greater than 5 at 2750-km depth, due to the pv-ppv phase transition. Although key thermodynamic properties of this phase transition are continually being updated (e.g. Catalli et al., 2009; Ammann et al., 2010; Grocholski et al., 2012), its likely presence in the deep mantle complicates interpretations of R: as noted by Karato and Karki (2001), in the presence of lower mantle phase transformations, high values of R do not necessarily imply chemical heterogeneity, as has previously been inferred.

3.6. Anti-correlations

Decompositions of shear and compressional wave velocity models into their shear and bulk-sound velocity contributions indicate that deep mantle LLSVPs may exhibit a negative correlation between shear wave and bulk-sound velocity anomalies (e.g. Su and Dziewonski, 1997; Kennett et al., 1998; Masters et al., 2000). As shear and bulk-moduli respond to temperature in the same way, this observation is commonly attributed to variations in bulk composition. However, correlations between shear and bulk-sound velocity anomalies from our models demonstrate that the inclusion of chemical heterogeneity does not produce a large-scale lower mantle anti-correlation. In all cases and away from phase transitions, synthetic models predict that V_P, V_S and V_ϕ structures are always highly correlated, with values near -1 or 1. In the lower mantle, only post-perovskite material, which occurs within $\sim$350-km of the CMB, produces a negative correlation between shear wave and bulk-sound velocity anomalies. Aside from this, they are positively correlated at all depths (Fig. 9). The thermodynamic compilation used predicts that under lower mantle conditions and relative to a pyrolite, basaltic material is slightly slower in bulk-sound but somewhat faster in shear wave velocity (within the post-perovskite stability field these effects are reversed), whereas iron-rich material is slower in both bulk-sound and shear wave velocity. At high temperatures near the CMB, this implies that no anti-correlation of bulk-sound and shear wave anomalies would be expected: in the basaltic case, the thermal effect on seismic velocity outweighs any chemical influence, whilst thermal and chemical effects enhance each other in the iron-rich case.

It should be noted that there is substantial disagreement between different seismic models on the depth, geographic location, extent and even existence of the shear-bulk-sound-velocity anti-correlation (e.g. Su and Dziewonski, 1997; Kennett et al., 1998; Masters et al., 2000; Malcolm and Trampert, 2011). For example, the study of Masters et al. (2000), which includes a wide range of data sensitive to deep mantle structure, shows a deep mantle anti-correlation that not only occurs inside LLSVPs, but also beneath the Americas and South-East Asia. This global trend appears to support the notion that observed shear-bulk-sound-velocity anti-correlations result from the pv-ppv phase transition. Due to the limited depth resolution of seismic studies, pv-ppv transition anomalies, like those observed here, may project into anti-correlations over larger depth ranges. Whilst this conjecture requires further testing, it does urge caution when interpreting correlations between different wave-speed anomalies. Indeed, like the ratio of shear and compressional wave-speed anomalies, V_S–V_ϕ correlations do not provide a simple way of distinguishing thermal from chemical mantle heterogeneity.

4. Discussion

We have compared the forward modelled seismic characteristics of synthetic thermal and thermo-chemical 'pile' mantle models. Our models are Earth-like in terms of convective vigour, surface heat flux and the geographic distribution of heterogeneity, which is controlled by the assimilated 300 MYr of plate motion history (Stampfli and Borel, 2002; Stampfli and Hochard, 2009). The most recent self-consistent lower mantle thermodynamic database is utilised when converting from physical to elastic structure (Stixrude and Lithgow-Bertelloni, 2011) and we include the effects of temperature-dependent anelasticity (Karato and Karki, 2001; Goes et al., 2004). Furthermore, we account for limited tomographic resolution when comparing to the tomographic model S40RTS (Ritsema et al., 2007, 2011). These steps are essential for generating synthetic structures that are directly comparable to seismic observations of Earth's present-day mantle.

Our results demonstrate that thermal heterogeneity alone can explain the amplitude and distribution of lower mantle shear wave velocity heterogeneity, thus corroborating the conclusions of Schuberth et al. (2009b,a). In addition, clusters of upwelling mantle plumes and interconnected hot, linear ridges, focussed beneath Africa and the Pacific by subduction history, can reconcile the major morphological characteristics of LLSVPs, without requiring a contribution from chemical heterogeneity. Anelastic seismic sensitivity to temperature ensures that temperature gradients of 800–1000 K/100 km, in and around these deep mantle structures, generate shear wave velocity gradients of 3.5–4.5%/100 km, which are comparable to those observed at the margins of LLSVPs (e.g. To et al., 2005; Schuberth et al., 2009a). Although higher velocity gradients are generated at the margins of chemical 'piles' in our thermo-chemical cases, deep mantle anomaly amplitudes are too strong in comparison to the S40RTS tomographic model. Our results also demonstrate that observed lower mantle ratios between shear and compressional wave-speed anomalies and anti-correlated shear and bulk-sound velocity anomalies are not easily explained by variations in bulk-composition: they are more likely related to the presence of post-perovskite. Taken together, this suggests that the seismic characteristics of LLSVPs do not require a substantial contribution from chemical heterogeneity.

Our inference that thermal variations dominate Earth's lower mantle seismic heterogeneity structure contrasts with conclusions from the majority of earlier studies (e.g. Tackley, 1998, 2002; McNamara and Zhong, 2005; Tan and Gurnis, 2007; Deschamps and Tackley, 2008, 2009; Bull et al., 2009), which warrants further discussion. Below we discuss the key differences between our models and those examined previously and how model limitations may affect results. We then highlight mineral physics and seismological uncertainties and end our discussion by considering the implications of results for the distribution of chemical heterogeneity within Earth's mantle.

4.1. Comparison with previous studies

Numerous studies have examined how thermo-chemical 'piles' might be reconciled with seismological constraints. For example, Deschamps and Tackley (2008, 2009) compare predictions from 3-D Cartesian convection simulations with the degree 2, 4, and 6 power spectra obtained in a probabilistic tomographic inversion

for thermal and compositional heterogeneity (Trampert et al., 2004). They argue that chemically dense 'piles', stable enough to be maintained over Earth's history, yet mobile enough to impose low-degree chemical heterogeneity throughout the lower mantle, are required to reproduce such spectra. In more recent work, this group use 3-D spherical models to explore the seismic signature of 'piles' formed by recycling oceanic lithosphere, focussing again on comparisons between models and spectral-amplitudes from tomography (e.g. Nakagawa et al., 2009, 2010). In a result compatible with ours, they find that for a range of possible basaltic properties, thermo-chemical 'piles' generate stronger lower-mantle heterogeneity than is imaged by seismic tomography. Furthermore, like us, they find that thermal effects dominate the seismic signature of basaltic material in the deep mantle. However, the aforementioned studies do not explicitly account for the limited resolving power of tomography and do not constrain the geographic pattern of heterogeneity using plate motion histories. As a result, they were unable to consistently compare the amplitudes of lower mantle heterogeneity with tomography.

Bull et al. (2009) were the first to compare the synthetic shear wave tomography of purely thermal and thermo-chemical 'pile' models, accounting for limited tomographic resolution using the resolution operator of S20RTS. They conclude that the power spectra of thermal and thermo-chemical 'pile' scenarios compare equally well to tomography. Nonetheless, they favour the thermo-chemical 'pile' scenario as it 'matches tomography better in visual comparison'. However, they do not quantitatively examine the amplitudes of lower mantle heterogeneity in either case, as is done here. Indeed, by doing so, we find that purely thermal models better resemble tomographically imaged structure. Whilst our numerical models are not too dissimilar to those of Bull et al. (2009), we include improvements that lead us to a different conclusion, the main change being that our models are compressible, which produces a larger range of thermal anomalies at depth. Although Bull et al. (2009) correct for compressibility by post-processing model output through the addition of a mantle adiabat, such a correction does not take into account the system's non-linearities and potential feedbacks between rheology, composition, viscous dissipation and adiabatic heating (e.g. Yuen et al., 1987). Other relevant differences are: (i) their synthetic structures do not include the anelastic contribution to seismic velocity anomalies; (ii) they omit the distinct seismic properties of post-perovskite; and (iii) they use the resolution filter of S20RTS, which, due to its longer wavelength nature (degree 20 as opposed to degree 40 in S40RTS), predicts more severely smoothed tomograms of the dynamic models, especially at the smaller scale of the purely thermal case. These factors would all lead to reduced seismic anomalies, particularly at depth, when compared to our synthetic structures.

In a different approach, Simmons et al. (2009, 2010) jointly invert seismic and geodynamic data, including the global free-air gravity field and plate motions, for the distribution of thermal and chemical heterogeneity within Earth's mantle. Although observed shear wave travel-times and geodynamic constraints can be reconciled without a significant contribution from chemical heterogeneity (Simmons et al., 2009), a small volume-fraction of chemical heterogeneity is required within LLSVPs to reconcile shear and compressional wave travel-time variations (Simmons et al., 2010). Studies that include constraints from normal modes and Earth's geoid agree with the latter conclusion (e.g. Ishii and Tromp, 1999; Masters et al., 2000; Trampert et al., 2004; Koelemeijer et al., 2012). However, more recent work questions whether the shear and compressional wave travel-time variations are a consequence of differential wave-front healing, as opposed to chemical heterogeneity (Malcolm and Trampert, 2011). Indeed, using a wave-propagation approach, which accounts for finite-frequency effects and avoids the problems of limited resolution and non-uniqueness inherent to tomographic inversions, Schuberth et al. (2012) demonstrate that thermal heterogeneity alone can account for the observed variance in long-period shear and compressional wave travel-times.

4.2. Modelling uncertainties

Although our models have many Earth-like characteristics, current constraints on key input parameters are not narrow enough to allow for the generation of a unique synthetic structure for a given conceptual model, whilst numerical considerations place restrictions on the complexity included. Our favouring of a mantle where the dynamics and large-scale seismic structure are predominantly thermally controlled hinges on a large enough range of thermal heterogeneity at depth. The model parameters that are of greatest relevance for lower mantle thermal heterogeneity include the CMB temperature and the magnitude of compressibility. Other important factors are the rheology, the depth-dependence of thermal conductivity and the post-perovskite phase transition.

A reduced CMB temperature would strongly decrease the range of thermal (and hence, seismic) anomalies at depth. Indeed, some previous studies prescribed a CMB temperature of ~ 3000 K (e.g. Kellogg et al., 1999), and inferred that the range of seismic anomalies generated at depth, in the absence of chemical heterogeneity, was insufficient to satisfy seismological constraints. However, recent results from geodynamics, seismology and mineral physics point towards a CMB temperature of 4000 ± 300K (e.g. Glatzmaier and Roberts, 1995; Kuang and Bloxham, 1997; Boehler, 2000; Alfè et al., 2002; Buffett, 2002; Gubbins et al., 2004; Nimmo et al., 2004; Hernlund et al., 2005; Nolet et al., 2006; Alfè et al., 2007; van der Hilst et al., 2007; Steinberger and Holme, 2008; Lay et al., 2008). It would therefore be difficult to defend the use of a CMB temperature that is substantially lower than the 4000 K prescribed herein.

Compressibility introduces additional sources and sinks of heat that are controlled by the dissipation number (Jarvis and McKenzie, 1980). In our simulations, surface and volume-averaged dissipation numbers are ~ 1.0 and ~ 0.5, respectively, consistent with estimates for Earth's mantle and values used in previous compressible mantle convection simulations (e.g. Tackley, 1996; Bunge et al., 1997; Tan and Gurnis, 2007; Deschamps and Tackley, 2008, 2009). Indeed, our reference density profile is in good agreement with the Preliminary Reference Earth Model (PREM) (Dziewonski and Anderson, 1981), whilst the depth dependence of our thermal expansion coefficient is consistent with lower mantle thermodynamic analyses (e.g. Chopelas and Boehler, 1992; Stixrude and Lithgow-Bertelloni, 2011).

We note that the parameters of our simulations are not fully self-consistent with the thermodynamic database utilised in converting from physical to seismic structure, the key difference being that we do not include the dynamic effects of the post-perovskite phase transition, which has been shown to de-stabilise the thermal boundary layer above the CMB (e.g. Nakagawa and Tackley, 2004; Tosi et al., 2010). In addition, our viscosity formulation is only mildly temperature dependent, with no dependence on composition or stress. Although slab sinking rates in our models are comparable to those observed tomographically (implying that, to first order, our formulation of mantle rheology is reasonable), the reduced temperature dependence means that our models do not capture the sharp reduction in viscosity that is predicted (e.g. Ammann et al., 2009, 2010) and is indeed observed (e.g. Peltier and Drummond, 2010; Nakada and Karato, 2012) within D″. Such low viscosities could destabilize the mantle's lower thermal boundary layer, thus modifying the distribution of

thermal (and seismic) heterogeneity at depth. However, as the effects are highly non-linear, quantifying exactly how this would influence our conclusions requires further modelling, in codes incorporating improved numerical solution strategies (e.g. Tackley, 2008; Davies et al., 2011). Nonetheless, studies by Deschamps and Tackley (2008, 2009) do demonstrate that a stronger temperature dependence and an increase in viscosity with composition both stabilise thermo-chemical 'piles', which would tend to enhance their seismic anomalies.

For simplicity, we assume a constant thermal conductivity of $4\ W\ m^{-1}\ K^{-1}$ in all models. However, thermal conductivity increases as a function of depth within Earth's mantle, most likely approaching values of 5.9–10 $W\ m^{-1}\ K^{-1}$ in the deep mantle (see Hofmeister, 2008; de Koker, 2010; Manthilake et al., 2011; Tackley, 2011; Hunt et al., 2012, for detailed discussion). In a test case, where conductivity increases linearly from a value of $4\ W\ m^{-1}\ K^{-1}$ at the surface to $8\ W\ m^{-1}\ K^{-1}$ at the CMB, we find that its inclusion only leads to a minor reduction in strength of deep mantle thermal anomalies, whilst their seismic expressions are not altered substantially from the reference case. This would suggest that the inclusion of a depth-dependent conductivity would not modify our conclusions.

Future work should test, in detail, the assumptions and approximations made in our models. Nonetheless, the models presented are based on a reasonable set of parameters and, with our current understanding of their sensitivity, it appears unlikely that lower mantle temperature anomalies would be reduced sufficiently to invalidate our conclusions that thermal heterogeneity alone can explain the key seismic observations of Earth's lower mantle, whereas the amplitude of seismic anomalies is over-predicted in thermo-chemical 'pile' cases. With that in mind, one could ask the question: is there any other means by which our thermo-chemical 'pile' model could be adjusted to reduce the amplitude of lower mantle heterogeneity? Although, for ease of presentation, we have focussed on comparisons between a single thermo-chemical 'pile' model and a purely thermal model, a suite of thermo-chemical cases have been examined, where the volume-fraction and excess density of chemical material is varied. As expected, models with a higher chemical density contrast yield more stable layers with less topography. Consistent with the predictions of Tackley (2002), we find that such global stratification generates very strong seismic heterogeneity at and around the chemical interface and also leads to sharp changes in one-dimensional radial velocity profiles, which are incompatible with seismic observations (e.g. Dziewonski and Anderson, 1981; Kennett et al., 1995). Thermo-chemical models with increased volume-fractions of dense material (of similar density contrast) produce 'piles' that cover a larger portion of the CMB and extend further into the mid-mantle, resulting in stronger deep mantle seismic anomalies and a radial distribution of heterogeneity that further decreases the correlation between thermo-chemical model predictions and imaged structure. Models with decreased volume-fractions of dense material or a lower chemical density contrast do reduce the amplitude of lowermost mantle heterogeneity. However, such models do not generate coherent thermo-chemical 'piles'. Taken together, this implies it is difficult to reconcile the shear wave velocity anomalies predicted from a thermo-chemical 'pile' scenario with seismological observations.

4.3. Mineral physics and seismological uncertainties

There are substantial uncertainties in extrapolating mineral properties to lower mantle pressure and temperature conditions. Indeed, estimates for the deep mantle temperature sensitivity of shear wave velocities range from a 3–6% change in V_S, per 1000 K (Cobden et al., 2009). The thermodynamic database and anelasticity model Q4 used here give temperature sensitivities towards the lower end of this range. A different set of parameters would thus further strengthen our conclusion that thermo-chemical 'piles' generate shear wave velocity anomalies that are too large in comparison to imaged velocities.

In addition, the lack of anti-correlation between bulk-sound and shear wave velocities under deep mantle conditions is reasonably robust, at least with our current knowledge of deep mantle mineral properties. Anti-correlated bulk-sound and shear wave velocity anomalies require that compositional effects dominate over thermal variations, which seems unlikely given the large thermal heterogeneity that we predict in the deep mantle. From all potential large-scale compositions that we have considered, only basaltic material has the high density necessary to make a long-lived 'pile', whilst also being a candidate for producing anti-correlations away from the post-perovskite phase transition (e.g. Cobden et al., 2009). A range of basaltic compositions have been proposed (e.g. Irifune and Ringwood, 1993; Ricolleau et al., 2010; Nakagawa et al., 2010), but all have significant proportions of calcium-perovskite and stishovite, when compared to a pyrolite. With the current data available, relative to a pyrolite, basaltic material is fast in shear wave velocity (due to the high shear wave velocities of calcium-perovskite and stishovite relative to magnesium-perovskite), but slightly slower in bulk-sound (due to its higher density, resulting from its high iron content, and the relatively similar bulk moduli of magnesium- and calcium-perovskite: Stixrude, pers. comm., 2011). As a result, one cannot attain a fast bulk-sound velocity, even at low thermal anomalies, and the hottest temperatures would need to be less than half of what we predict to have compositional effects on shear wave velocity outweigh thermal effects (note also that this is with anelasticity model Q4, which has a relatively low temperature sensitivity). Even if basaltic material was fast in bulk-sound velocity, in comparison to a pyrolite, the temperature anomalies generated in our models would easily counteract this. We emphasize that we cannot rule out compositions very different from those considered here being sequestered in the deep mantle, whilst additional complexity may be introduced by iron spin transitions under lower mantle conditions (e.g. Badro et al., 2003, 2004; Crowhurst et al., 2008). However, with our current knowledge of mineral properties, phase relations and likely mantle compositions, none generate anti-correlated seismic velocity anomalies at the expected deep-mantle thermal anomalies, except within the post-perovskite stability field.

Limited seismic resolution may result in smearing such anti-correlated post-perovskite properties over a larger depth range, and this conjecture should be tested in a future study. However, the pressure and temperature conditions of the post-perovskite phase boundary remain the subject of ongoing debate. A recent paper by Grocholski et al. (2012) finds that the stability of the post-perovskite phase strongly depends on the bulk chemical composition, concluding that in a pyrolite-like mantle, the post-perovskite phase would not appear at any relevant pressure and temperature conditions. If correct, the only possible explanation for the observed anti-correlation between shear and bulk-sound velocity anomalies (and elevated ratios between shear and compressional wave-speed anomalies), in a mantle without substantial large-scale chemical heterogeneity, would be that it is an artefact from the effects of wavefront healing (Malcolm and Trampert, 2011; Schuberth et al., 2012).

We note that our models should be further tested against density sensitive data, such as normal-modes (although these do form part of the S40RTS data-set) and the geoid. In several inversions, such data have required an anti-correlation between shear wave velocity and density (e.g. Ishii and Tromp, 1999; Trampert et al., 2004; Koelemeijer et al., 2012), which our work

confirms does require compositional heterogeneity. However, other studies demonstrate that the constraints from these datasets for high-density deep mantle 'piles' may not be strong (e.g. Romanowicz, 2001; Simmons et al., 2009), whilst comparisons between simple isochemical mantle convection scenarios and the observed geoid are already in close agreement (e.g. Ricard et al., 2006).

4.4. The likely distribution of chemical heterogeneity within Earth's mantle

A chemically heterogeneous mantle is an unavoidable consequence of plate tectonics. It is also essential to satisfy a wide-range of geochemical constraints on mantle structure (e.g. De Paolo and Wasserburg, 1976; Zindler and Hart, 1986; Allègre et al., 1996; Hofmann, 1997, 2003; Labrosse et al., 2007). Although our isochemical model provides an excellent match to the seismological observations examined herein, we are not advocating an isochemical mantle. However, our results imply that geochemical reservoirs, in the form of large-scale deep mantle 'piles', are likely incompatible with seismological constraints on mantle structure, limiting the likely volume-fractions of dense material that can be sequestered in such regions to $\ll 3\%$. Our results however, do not rule out more distributed small-scale heterogeneity, or a chemically heterogeneous D″. Indeed, several studies now argue that large-scale source regions may not be required to explain the geochemical diversity of MORBs and OIBs (e.g. Helffrich and Wood, 2001; Davies, 2009, 2010). A smaller-scale reservoir within D″ (e.g. Coltice and Ricard, 1999), combined with distributed heterogeneity throughout the lower mantle (e.g. Helffrich and Wood, 2001), could potentially satisfy key geochemical constraints on mantle structure. However, we stress that this conjecture requires careful testing in a fully dynamic model, which includes the recycling of oceanic plates and the evolution of geochemical tracers, as has previously been done for thermo-chemical 'pile' models (e.g. Tackley and Xie, 2002; Xie and Tackley, 2004a,b; Brandenburg and van Keken, 2007; Brandenburg et al., 2008).

5. Conclusions

By comparing the forward modelled seismic characteristics of synthetic thermal and thermo-chemical 'pile' mantle structures with a range of seismological observations, we demonstrate that:

1. Temperature variations alone can explain the amplitude and distribution of shear wave velocity heterogeneity in the deep mantle.
2. Plume clusters and interconnected hot, linear ridges, naturally focussed beneath Africa and the Pacific by plate motion histories, can reconcile the major morphological characteristics of LLSVPs.
3. Chemical heterogeneity need not be invoked to explain rapid variations in seismic velocity observed at the margins of deep mantle LLSVPs.
4. Thermo-chemical 'pile' models, where dense chemical heterogeneity is concentrated into large-scale structures beneath Africa and the Pacific, over-predict deep mantle anomaly amplitudes when compared to the shear wave tomography model S40RTS, even after accounting for the geographic bias, smearing and damping inherent to the tomographic inversion. The radial distribution of heterogeneity in such cases also differs from the tomographic model.
5. In the presence of post-perovskite, ratios between shear and compressional wave-speed anomalies, or correlations between shear and bulk-sound velocity anomalies, cannot conclusively distinguish thermal from chemical heterogeneity in the lowermost mantle.

Taken together, our findings suggest that lower mantle LLSVPs are dominantly thermal structures, arising naturally from vigorous whole mantle convection, with the geographic distribution of heterogeneity dictated by plate motion histories. Such plate motions can explain the relative fixity of these deep mantle provinces on a several hundred million year time scale (e.g. Burke and Torsvik, 2004), without requiring a contribution from chemical density.

Geochemical constraints and the continuous recycling of oceanic plates preclude an isochemical mantle. Indeed, given the uncertainties associated with extrapolating mineral properties to deep mantle conditions and the approximations inherent to our models, our results cannot rule out some accumulation of chemical heterogeneity in the deep mantle beneath Africa and the Pacific. However, they do imply that only small volume-fractions ($\ll 3\%$ of the mantle's volume) of concentrated dense material can be accommodated in these regions. Any additional heterogeneity, which may be required to satisfy geochemical constraints on mantle structure, must therefore be distributed elsewhere in the mantle. This, in turn, implies that compositional heterogeneity is dynamically and seismically less significant than has previously been inferred.

Acknowledgements

D.R.D. was funded by Fellowships from the Royal Commission for the Great Exhibition of 1851 and NERC (NE/H015329/1). B.S.A.S. was supported by a Marie Curie Intra European Fellowship within the 7th European Community Framework Programme (FP7/2007-2013), under grant agreement number 235861. Numerical simulations were undertaken at: (i) HECToR, the UK's national high-performance computing service, which is provided by UoE HPCx Ltd at the University of Edinburgh, Cray Inc and NAG Ltd, and funded by the Office of Science and Technology through EPSRC's High End Computing Program; (ii) the Imperial College High Performance Computing centre; and (iii) ARCCA, at Cardiff University. D.R.D. would like to thank: (i) Lars Stixrude and Carolina Lithgow-Bertelloni for providing the lookup tables used in converting models from physical structure to seismic velocity; (ii) Cyril Hochard, Gerard Stampfli and Peter Webb for support in implementing and testing the plate history model utilised; and (iii) Ian Merrick, Cian Wilson and Stephan Kramer for support with visualisation. Authors would like to thank Paul Tackley, Yanick Ricard and two anonymous reviewers for constructive and thorough comments during the review process.

Appendix A. Supplementary data

Supplementary data associated with this article can be found in the online version at http://dx.doi.org/10.1016/j.epsl.2012.08.016.

References

Alfè, D., Gillan, M.J., Price, G.D., 2007. Temperature and composition of the Earth's core. Contemp. Phys. 48, 63–80.
Alfè, D., Price, G.D., Gillan, M.J., 2002. Iron under Earth's core conditions: liquid–state thermodynamics and high-pressure melting curve from ab initio calculations. Contemp. Phys. B 65, 165118–165129.
Allègre, C.J., Hofmann, A.W., O'Nions, R.K., 1996. The Argon constraints on mantle structure. Geophys. Res. Lett. 23, 3555–3557.

Ammann, M.W., Brodholt, J.P., Dobson, D.P., 2009. DFT study of migration enthalpies in $MgSiO_3$ perovskite. Phys. Chem. Minerals 36, 151–158.
Ammann, M.W., Brodholt, J.P., Wookey, J., Dobson, D.P., 2010. First-principles constraints on diffusion in lower-mantle minerals and a weak D″ layer. Nature 465, 251–267.
Badro, J., Fiquet, G., Guyot, F., Rueff, J., Struzhkin, V.V., Vankó, G., Monaco, G., 2003. Iron partitioning in Earth's mantle: toward a deep lower-mantle discontinuity. Science 300, 789–791.
Badro, J., Rueff, J., Vankó, G., Monaco, G., Fiquet, G., Guyot, F., 2004. Electronic transitions in perovskite: possible non-convecting layers in the lower mantle. Science 305, 383–386.
Baumgardner, J.R., 1985. Three-dimensional treatment of convective flow in the Earth's mantle. J. Stat. Phys. 39, 501–511.
Becker, T.W., Boschi, L., 2002. A comparison of tomographic and geodynamic mantle models. Geochem. Geophys. Geosys. 3, 5555, Paper number 2001GC000168.
Boehler, R., 2000. High-pressure experiments and the phase diagram of lower mantle and core materials. Rev. Geophys. 38, 221–245.
Brandenburg, J.P., Hauri, E.H., van Keken, P.E., Ballentine, C.J., 2008. A multiple-system study of the geochemical evolution of the mantle with force-balanced plates and thermochemical effects. Earth Planet. Sci. Lett. 276, 1–13.
Brandenburg, J.P., van Keken, P.E., 2007. Deep storage of oceanic crust in a vigorously convecting mantle. J. Geophys. Res. 112, B06403.
Brodholt, J.P., Hellfrich, G., Trampert, J., 2007. Chemical versus thermal heterogeneity in the lower mantle: the most likely role of anelasticity. Earth Planet. Sci. Lett. 262, 429–437.
Buffett, B.A., 2002. Estimates of heat flow in the deep mantle based on the power requirements for the geodynamo. Geophys. Res. Lett. 29, 4PP.
Bull, A.L., McNamara, A.K., Ritsema, J., 2009. Synthetic tomography of plume clusters and thermochemical piles. Earth Planet. Sci Lett. 278, 152–156.
Bunge, H.-P., 2005. Low plume excess temperature and high core heat flux inferred from non-adiabatic geotherms in internally heated mantle circulation models. Phys. Earth Planet. Int. 153, 3–10.
Bunge, H.-P., Richards, M.A., Baumgardner, J.R., 1997. A sensitivity study of 3-D-spherical mantle convection at 10^8 Rayleigh number: effects of depth-dependent viscosity, heating mode and an endothermic phase change. J. Geophys. Res. 102, 11991–12007.
Bunge, H.-P., Richards, M.A., Lithgow-Bertelloni, C., Baumgardner, J.R., Grand, S., Romanowicz, B., 1998. Time scales and heterogeneous structure in geodynamic Earth models. Science 280, 91–95.
Burke, K., Steinberger, B., Torsvik, T.H., Smethurst, M.A., 2008. Plume generation zones at the margins of large low shear velocity provinces on the core–mantle-boundary. Earth Planet. Sci. Lett. 265, 49–60.
Burke, K., Torsvik, T.H., 2004. Derivation of large igneous provinces of the past 200 million years from long-term heterogeneities in the deep mantle. Earth Planet. Sci. Lett. 227, 531–538.
Cammarano, F., Goes, S., Vacher, P., Giardini, D., 2003. Inferring upper-mantle temperatures from seismic velocities. Phys. Earth Planet. Int. 138, 197–222.
Catalli, K., Shim, S., Prakapenka, V., 2009. Thickness and Clapeyron slope of the post-perovskite boundary. Nature 462, 782–785.
Chopelas, A., Boehler, R., 1992. Thermal expansivity in the lower mantle. Geophys. Res. Lett. 19, 1983–1986.
Christensen, U.R., Hofmann, A.W., 1994. Segregation of subducted oceanic crust in the mantle. J. Geophys. Res. 99, 19867–19884.
Cobden, L., Goes, S., Ravenna, M., Styles, E., Cammarano, F., Gallagher, K., Connolly, J.A.D., 2009. Thermochemical interpretation of 1-D seismic data for the lower mantle: the significance of non-adiabatic thermal gradients and compositional heterogeneity. J. Geophys. Res. 114, B11309.
Coltice, N., Ricard, Y., 1999. Geochemical observations and one layer mantle convection. Earth Planet. Sci. Lett. 174, 125–137.
Crowhurst, J.C., Brown, J.M., Goncharov, A.F., Jacobsen, S.D., 2008. Elasticity of (Mg,Fe)O through the spin transition of Iron in the lower mantle. Science 319, 451–453.
Davaille, A., 1999. Simultaneous generation of hotspots and superswells by convection in a heterogeneous planetary mantle. Nature 402, 756–760.
Davies, D.R., Davies, J.H., 2009. Thermally-driven mantle plumes reconcile multiple hot-spot observations. Earth Planet. Sci. Lett. 278, 50–54.
Davies, D.R., Wilson, C.R., Kramer, S.C., 2011. Fluidity: a fully unstructured anisotropic adaptive mesh computational modeling framework for geodynamics. Geochem. Geophys. Geosys. 120, Q06001.
Davies, G.F., 1999. Dynamic Earth: Plates, Plumes and Mantle Convection. Cambridge University Press.
Davies, G.F., 2009. Reconciling the geophysical and geochemical mantles: plume flows, heterogeneities and disequilibrium. Geochem. Geophy. Geosyst. 10, Q10008.
Davies, G.F., 2010. Noble gases in the dynamic mantle. Geochem. Geophys. Geosyst. 11, Q03005.
Davies, J.H., Bunge, H.P., 2001. Seismically 'fast' geodynamic mantle models. Geophys. Res. Lett. 28, 73–76.
de Koker, N., 2010. Thermal conductivity of MgO at high pressure: implications for the D″ region. Earth Planet. Sci. Lett. 292, 392–398.
De Paolo, D.J., Wasserburg, G.J., 1976. Inferences about magma sources and mantle structure from variations of $^{143}Nd/^{144}Nd$. Geophys. Res. Lett. 3, 743–746.
Della Mora, S., Boschi, L., Tackley, P.J., Nakagawa, T., Giardini, D., 2011. Low seismic resolution cannot explain S/P decorrelation in the lower mantle. Geophys. Res. Lett. 38, 5555.
Deschamps, F., Tackley, P.J., 2008. Exploring the model space of thermo-chemical convection: (i) principles and influence of the rheological parameters. Phys. Earth Planet. Int. 171, 357–373.
Deschamps, F., Tackley, P.J., 2009. Searching for models of thermo-chemical convection that explain probabilistic tomography: (ii) influence of physical and compositional parameters. Phys. Earth Planet. Int. 176, 1–18.
Duncan, R.A., Richards, M.A., 1991. Hotspots, mantle plumes, flood basalts and true polar wander. Rev. Geophys. 29, 31–50.
Dziewonski, A.M., Anderson, D.L., 1981. Preliminary reference Earth model. Phys. Earth. Planet. Int. 25, 297–356.
Garnero, E.J., Lay, T., McNamara, A., 2007. Implications of lower-mantle structural heterogeneity for existence and nature of whole-mantle plumes. Geol. Soc. Am. Spec. Publ. 430, 79–88.
Glatzmaier, G.A., Roberts, P.H., 1995. A 3-dimensional self-consistent computer simulation of a geomagnetic field reversal. Nature 377, 203–209.
Goes, S., Cammarano, F., Hansen, U., 2004. Synthetic seismic signature of thermal mantle plumes. Earth Planet. Sci. Lett. 218, 403–419.
Grand, S., van der Hilst, R.D., Widiyantoro, S., 1997. Global seismic tomography: a snapshot of mantle convection in the Earth. GSA Today 7, 1–7.
Grocholski, B., Catalli, K., Shim, S.-H., Prakapenka, V., 2012. Mineralogical effects on the detectability of the post-perovskite boundary. Proc. Nat. Acad. Sci., http://dx.doi.org/10.1073/pnas.1109204109.
Gubbins, D., Alfè, D., Masters, G., Price, G.D., Gillan, M., 2004. Gross thermodynamics of two-component core convection. Geophys. J. Int. 157, 1407–1414.
Gurnis, M., Mitrovica, J.X., Ritsema, J., van Heijst, H.J., 2000. Constraining mantle density structure using geological evidence of surface uplift rates: the case of the African superplume. Geochem. Geophys. Geosys. 1 1999GC000035.
Hager, B.H., Clayton, R.W., Richards, M.A., Comer, R.P., Dziewonski, A.M., 1985. Lower mantle heterogeneity, dynamic topography and the geoid. Nature 313, 541–545.
He, Y., Wen, L., 2009. Structural features and shear-velocity structure of the 'Pacific anomaly'. J. Geophys. Res 114.
Helffrich, G.R., Wood, B.J., 2001. The Earth's mantle. Nature 412, 501–507.
Hernlund, J.W., Houser, C., 2008. On the statistical distribution of seismic velocities in Earth's deep mantle. Earth Planet. Sci. Lett. 265, 423–437.
Hernlund, J.W., Thomas, C., Tackley, P.J., 2005. A doubling of the post-perovskite phase boundary and structure of the Earth's lowermost mantle. Nature 434, 882–886.
Herzberg, C., Asimow, P.D., Arndt, N., Niu, Y., Lesher, C.M., Fitton, J.G., Cheadle, M.J., Saunders, A.D., 2007. Temperatures in ambient mantle and plumes: constraints from basalts, picrites, and komatiites. Geochem. Geophys. Geosys. 8, 397–403.
Hofmann, A.W., 1997. Mantle geochemistry: the message from oceanic volcanism. Nature 385, 219–229.
Hofmann, A.W., 2003. Sampling mantle heterogeneity through oceanic basalts: isotopes and trace elements. In: Treatise on Geochemistry. Elsevier, pp. 61–101.
Hofmeister, A.M., 2008. Inference of high thermal transport in the lower mantle from laser-flash experiments and the damped harmonic oscillator model. Phys. Earth Planet. Int. 170.
Houser, C., Masters, G., Shearer, P., Laske, G., 2008. Shear and compressional velocity models of the mantle from cluster analysis of long-period waveforms. Geophys. J. Int. 174, 195–212.
Hunt, S.A., Davies, D.R., Walker, A.M., McCormack, R.J., Wills, A.S., Dobson, D.P., Li, L., 2012. On the increase in thermal diffusivity caused by the perovskite to post-perovskite phase transition and its implications for mantle dynamics. Earth Planet. Sci. Lett. 319, 96–103.
Irifune, T., Ringwood, A.E., 1993. Phase transformations in subducted oceanic crust and buoyancy relationships at depths of 600–800 km in the mantle. Earth Planet. Sci. Lett. 117, 101–110.
Ishii, M., Tromp, J., 1999. Normal-mode and free-air gravity constraints on lateral variations in velocity and density of Earth's mantle. Science 285, 1231–1236.
Jarvis, G.T., McKenzie, D.P., 1980. Convection in a compressible fluid with infinite Prandtl number. J. Fluid Mech. 96, 515–583.
Jeanloz, R., Morris, S., 1987. Is the mantle geotherm sub-adiabatic? Geophys. Res. Lett. 143, 335–338.
Karato, S.-I., 1993. The importance of anelasticity in the interpretation of seismic tomography. Geophys. Res. Lett. 20, 1623–1626.
Karato, S.-I., Karki, B.B., 2001. Origin of lateral variation of seismic wave velocities and density in the deep mantle. J. Geophys. Res. 106, 21771–21783.
Kellogg, L.H., Hager, B.H., van der Hilst, R.D., 1999. Compositional stratification in the deep mantle. Science 283, 1881–1884.
Kennett, B.L.N., Engdahl, R., Buland, R., 1995. Constraints on seismic velocities in the Earth from travel-times. Geophys. J. Int. 122, 108–124.
Kennett, B.L.N., Widiyantoro, S., van der Hilst, R.D., 1998. Joint seismic tomography for bulk sound and shear wave speed in the Earth's mantle. J. Geophys. Res. 103, 12469–12493.
Koelemeijer, P.J., Deuss, A., Trampert, J., 2012. Normal mode sensitivity to Earth's D″ layer and topography on the core–mantle-boundary: what we can and cannot see. Geophys. J. Int. 190.
Kuang, W.L., Bloxham, J., 1997. An Earth-like numerical dynamo model. Nature 289, 371–374.
Labrosse, S., Hernlund, J.W., Coltice, N., 2007. A crystallizing dense magma ocean at the base of Earth's mantle. Nature 450, 866–869.

Lay, T., Hernlund, J., Buffett, B.A., 2008. Core–mantle-boundary heat flow. Nat. Geo. 1.
Lay, T., Hernlund, J., Garnero, E.J., Thorne, M.S., 2006. A post-perovskite lens and D″ heat flux beneath the Central Pacific. Science 314.
Leng, W., Zhong, S., 2008. Controls on plume heat flux and plume excess temperature. J Geophys. Res. 113.
Malcolm, A.E., Trampert, J., 2011. Tomographic errors from wave front healing: more than just a fast bias. Geophys. J. Int. 185, 385–402.
Manthilake, M.A.G.M., de Koker, N., Frost, N., McCammon, D.J., 2011. Lattice thermal conductivity of lower mantle minerals and heat flux from Earth's core. Proc. Nat. Acad. Sci. 108, 17901–17904.
Masters, G., Laske, G., Bolton, H., Dziewonski, A.M., 2000. and compressional velocity in the mantle: implications for chemical and thermal structure. AGU Monograph, Earth's Deep Interior 171, 63–87.
Matas, J., Bukowinski, M.S.T., 2007. On the anelastic contribution to the temperature dependence of lower mantle seismic velocities. Earth Planet. Sci. Lett. 259, 51–65.
McNamara, A.K., Zhong, S., 2005. Thermo-chemical structures beneath Africa and the Pacific Ocean. Nature 437, 1136–1139.
Mégnin, C., Bunge, H.-P., Romanowicz, B., Richards, M.A., 1997. Imaging 3-D spherical convection models: what can seismic tomography tell us about mantle dynamics? Geophys. Res. Lett. 24, 1299–1302.
Murakami, M., Hirose, K., Kawamura, K., Sata, N., Ohishi, Y., 2004. Post-perovskite phase transition in $MgSiO_3$. Science 304, 855–858.
Nakada, M., Karato, S.-I., 2012. Low viscosity of the bottom of the Earth's mantle inferred from the analysis of Chandler wobble and tidal deformation. Phys. Earth Planet. Int. 192, 68–80.
Nakagawa, T., Tackley, P.J., 2004. Effects of a perovskite–post perovskite phase change near core–mantle-boundary in compressible mantle convection. Geophys. Res. Lett. 31, L16611.
Nakagawa, T., Tackley, P.J., 2006. Three-dimensional structures and dynamics in the deep mantle: effects of a post-perovskite phase change and deep mantle layering. Geophys. Res. Lett. 33.
Nakagawa, T., Tackley, P.J., Deschamps, F., Connolly, J.A.D., 2009. Incorporating self-consistently calculated mineral physics into thermo-chemical mantle convection simulations in a 3-D spherical shell and its influence on seismic anomalies in Earth's mantle. Geochem. Geophys. Geosys. 10, Q3304.
Nakagawa, T., Tackley, P.J., Deschamps, F., Connolly, J.A.D., 2010. The influence of MORB and Harzburgite composition on thermo-chemical mantle convection in a 3D spherical shell with self-consistently calculated mineral physics. Earth Planet. Sci. Lett. 296, 403–412.
Ni, S.D., Helmburger, D.V., 2003. Ridge-like lower mantle structure beneath South Africa. J. Geophys. Res. 108, 2094–3008.
Ni, S.D., Tan, E., Gurnis, M., Helmberger, D.V., 2002. Sharp sides to the African superplume. Science 296, 1850–1852.
Nimmo, F., Price, G.D., Brodholt, J., Gubbins, D., 2004. The influence of Potassium on core and geodynamo evolution. Geophys. J. Int. 156, 363–376.
Nolet, G., Karato, S.-I., Montelli, R., 2006. Plume fluxes from seismic tomography. Earth Planet. Sci. Lett. 248, 685–699.
Nyblade, A.A., Robinson, S.W., 1994. The African superswell. Geophys. Res. Lett. 21, 765–768.
Oganov, A.R., Ono, S., 2004. Theoretical and experimental evidence for a post–perovskite phase of $MgSiO_3$ in Earth's D″ layer. Nature 430, 445–448.
Parmentier, E.M., Sotin, C., Travis, B.J., 1994. Turbulent, 3-D thermal convection in an infinite Prandtl number, volumetrically heated fluid: implications for mantle dynamics. Geophys. Res. Lett. 116, 241–251.
Peltier, W.R., Drummond, R., 2010. Deepest mantle viscosity: constraints from Earth rotation anomalies. Geophys. Res. Lett. 37, L12304.
Ricard, Y., Chambat, F., Lithgow-Bertelloni, C., 2006. Gravity observations and 3-D structure of the earth. C. R. Geosci. 338, 992–1001.
Ricolleau, A., Perrillat, J.P., Fiquet, G., Daniel, I., Matas, J., Addad, A., Menguy, N., Cardon, H., Mezouar, M., Guignot, N., 2010. Phase relations and equation of state of a natural morb: implications for the density profile of subducted oceanic crust in the Earth's lower mantle. J. Geophys. Res. 115, B08202.
Ritsema, J., McNamara, A.K., Bull, A., 2007. Tomographic filtering of geodynamic models: implications for model interpretation and large-scale mantle structure. J. Geophys. Res. 112.
Ritsema, J., Ni, S., Helmberger, D.V., Crotwell, H.P., 1998. Evidence for strong shear velocity reductions and velocity gradients in the lower mantle beneath africa. Geophys. Res. Lett. 25, 4245–4248.
Ritsema, J., van Heijst, H.J., 2002. Constraints on the correlation of P- and S-wave velocity heterogeneity in the mantle from Pbb PPbb PPP and PKPab traveltimes. Geophys. J. Int. 149, 482–489.
Ritsema, J., van Heijst, H.J., Deuss, A., Woodhouse, J.H., 2011. S40RTS a Degree-40 shear velocity model for the mantle from new Rayleigh wave dispersion, teleseismic traveltimes, and normal-mode splitting function measurements. Geophys. J. Int. 184, 1223–1236.
Robertson, G.S., Woodhouse, J.H., 1995. Evidence for proportionality of P and S heterogeneity in the lower mantle. Geophys. J. Int. 123, 85–116.
Romanowicz, B., 2001. Can we resolve 3-D density heterogeneity in the lower mantle? Geophys. Res. Lett. 28, 1107–1110.
Saltzer, R.L., van der Hilst, R.D., Karason, H., 2001. Comparing P and S wave heterogeneity in the mantle. Geophys. Res. Lett. 28, 1335–1338.
Schilling, J.G., 1991. Fluxes and excess temperatures of mantle plumes inferred from their interaction with migrating mid-ocean ridges. Nature 352, 397–403.
Schuberth, B.S.A., Bunge, H.-P., Ritsema, J., 2009a. Tomographic filtering of high-resolution mantle circulation models: can seismic heterogeneity be explained by temperature alone? Geochem. Geophys. Geosyst. 10, Q05W03.
Schuberth, B.S.A., Bunge, H.-P., Steinle-Neumann, G., Moder, C., Oeser, J., 2009b. Thermal versus elastic heterogeneity in high-resolution mantle circulation models with pyrolite composition: high plume excess temperatures in the lowermost mantle. Geochem. Geophy. Geosyst. 10, Q01W01.
Schuberth, B.S.A., Zaroli, C., Nolet, G., 2012. Synthetic seismograms for a synthetic Earth: long-period P- and S-wave traveltime variations can be explained by temperature alone. Geophys. J. Int. 200, 1393–1412.
Sidorin, I., Gurnis, M., Helmberger, D.V., 1999. Evidence for a ubiquitous seismic discontinuity at the base of the mantle. Science 286, 1326–1331.
Simmons, N.A., Forte, A.M., Boschi, L., Grand, S.P., 2010. GyPSuM: a joint tomographic model of mantle density and seismic wave speeds. J. Geophys. Res. 115, 5555.
Simmons, N.A., Forte, A.M., Grand, S.P., 2009. Joint seismicbb geodynamic and mineral physical constraints on three-dimensional mantle heterogeneity: implications for the relative importance of thermal versus compositional heterogeneity. Geophys. J. Int 177, 1284–1304.
Stampfli, G.M., Borel, G.D., 2002. A plate tectonic model for the Paleozoic and Mesozoic constrained by dynamic plate boundaries and restored synthetic oceanic isochrons. Earth Planet. Sci. Lett. 196, 17–33.
Stampfli, G.M., Hochard, C., 2009. Plate tectonics of the Alpine realm. Geol. Soc. London Spec. Publ. 327, 89–111.
Stegman, D.R., Jellinek, A.M., Zatman, S.A., Baumgardner, J.R., Richards, M.A., 2003. An early lunar core dynamo driven by thermo-chemical mantle convection. Nature 421, 143–146.
Steinberger, B., Holme, R., 2008. Mantle flow models with core–mantle-boundary constraints and chemical heterogeneities in the lowermost mantle. J. Geophys. Res 113, 5555.
Stixrude, L., Lithgow-Bertelloni, C., 2005. Thermodynamics of mantle minerals—i. Physical properties. Geophys. J. Int. 162, 610–632.
Stixrude, L., Lithgow-Bertelloni, C., 2007. Influence of phase transformations on lateral heterogeneity and dynamics in Earth's mantle. Earth Planet. Sci. Lett. 263, 45–55.
Stixrude, L., Lithgow-Bertelloni, C., 2011. Thermodynamics of mantle minerals—ii. Phase equilibria. Geophys. J. Int. 184, 1180–1213.
Styles, E., Davies, D.R., Goes, S., 2011. Mapping spherical seismic into physical structure: biases from 3-D phase-transition and thermal boundary-layer heterogeneity. Geophys. J. Int. 184, 1371–1378.
Su, W.J., Dziewonski, A.M., 1997. Simultaneous inversion for 3-D variations in shear and bulk velocity in the mantle. Phys. Earth Planet. Int. 100, 135–156.
Tackley, P.J., 1996. Effects of strongly variable viscosity on three-dimensional compressible convection in planetary mantles. J. Geophys. Res. 101, 3311–3332.
Tackley, P.J., 1998. Three-dimensional simulation of mantle convection with a thermo-chemical boundary layer: D″? In: Gurnis, M., Wysession, M.E., Knittle, E., Buffet, B.A. (Eds.), The core–mantle-boundary region. AGU, Washington DC, pp. 231–253.
Tackley, P.J., 2002. Strong heterogeneity caused by deep mantle layering. Geochem. Geophys. Geosys. 3, 1024.
Tackley, P.J., 2008. Modelling compressible mantle convection with large viscosity contrasts in a three-dimensional spherical shell using the Yin-Yang grid. Phys. Earth Planet. Int. 171, 7–18.
Tackley, P.J., 2011. Dynamics and evolution of the deep mantle resulting from thermal, chemical, phase and melting effects. Earth Sci. Rev. 110, 1–25.
Tackley, P.J., King, S.D., 2003. Testing the tracer ratio method for modelling active compositional fields in mantle convection simulations. Geochem. Geophys. Geosys 4, 8302.
Tackley, P.J., Xie, S., 2002. The thermo-chemical structure and evolution of Earth's mantle: constraints and numerical models. Phil. Trans. R. Soc. London A. 360, 2593–2609.
Tan, E., Gurnis, M., 2007. Compressible thermochemical convection and application to lower mantle structures. J. Geophys. Res. 112, B06304.
Thorne, M.S., Garnero, E.J., Grand, S.P., 2004. Geographic correlation between hot spots and deep mantle lateral shear-wave velocity gradients. Phys. Earth Planet. Int. 146, 47–63.
To, A., Romanowicz, B., Capdeville, Y., Takeuchi, N., 2005. 3-D effects of sharp boundaries at the borders of the African and Pacific superplumes: observation and modeling. Earth Planet. Sci. Lett. 233, 137–153.
Tosi, N., Yuen, D.A., Cadek, O., 2010. Dynamical consequences in the lower mantle with the post-perovskite phase change and strongly depth-dependent thermodynamic and transport properties. Earth Planet. Sci. Lett. 298, 229–243.
Trampert, J., Deschamps, F., Resovsky, J., Yuen, D., 2004. Probabilistic tomography maps chemical heterogeneities throughout the lower mantle. Science 306, 853–856.
van der Hilst, R.D., de Hoop, M.V., Wang, P., Shim, S.H., Ma, P., Tenorio, L., 2007. Seismostratigraphy and thermal structure of Earth's core–mantle-boundary region. Science 315, 1813–1817.
van der Hilst, R.D., Widiyantoro, S., Engdahl, E.R., 1997. Evidence for deep mantle circulation from global tomography. Nature 386, 578–584.
van Keken, P.E., Hauri, E., Ballentine, C.J., 2002. Mantle mixing: the generation, preservation and destruction of chemical heterogeneity. Annu. Rev. Earth Planet. Sci. 30, 493–525.
Wang, Y., Wen, L., 2007. Geometry and P and S velocity structure of the 'African anomaly'. J. Geophys. Res. 112.
Wolstencroft, M., Davies, J.H., Davies, D.R., 2009. Nusselt–Rayleigh number scaling for spherical shell Earth mantle simulation up to a Rayleigh number of 10^9. Phys. Earth Planet. Int. 176, 132–141.

Wookey, J., Stackhouse, S., Kendall, J., Brodholt, J., Price, G.D., 2005. Efficacy of the post-perovskite phase as an explanation for lowermost-mantle seismic properties. Nature 438, 1004–1007.
Xie, S., Tackley, P.J., 2004a. Evolution of helium and argon isotopes in a convecting mantle. Phys. Earth. Planet. Int. 146, 417–439.
Xie, S., Tackley, P.J., 2004b. Evolution of U-Pb and Sm-Nd systems in numerical models of mantle convection. J. Geophys. Res. 109.
Yuen, D.A., Quareni, F., Hong, H.J., 1987. Effects from equation of state and rheology in dissipative heating in compressible mantle convection. Nature 326, 67–69.
Zindler, A., Hart, S., 1986. Chemical geodynamics. Ann. Rev. Earth Planet. Sci. 14, 493–571.